Forschungszentrum Karlsruhe

Technik und Umwelt

Wissenschaftliche Berichte

FZKA 6366

Modeling of the Anode Plasma in Applied-B Ion Diodes

I.S. Landman*, H. Würz

Institut für Hochleistungsimpuls- und Mikrowellentechnik

* permanent address: Troitsk Institute for Innovation and Fusion Research, 142092 Troitsk, Russia

Forschungszentrum Karlsruhe GmbH, Karlsruhe

1999

This work partly was supported in the frame of the Russian German WTZ cooperation agreement RUS-524-96

Abstract

A model describing formation and evolution of the anode plasma in the accelerating gap of an applied-B ion diode is developed. Ionization processes in the gap and hydrogen release from a Ti-Pd film are included. The developed model was used to analyze the quasineutral layer containing a self-consistent electric field and the pre-anode electrostatic sheath from which the ion beam is extracted. Electron diffusion from the cathode is assumed to be anomalous resulting in homogeneous electron density over the main volume of the gap. Scenario calculations have been carried out for diode voltages rising from zero up to several million volts and operation times of several tenths of nanoseconds. For the analysis an analytical and a 2 dim numerical model are used. Regimes are found with complete exhaustion of the quasineutral layer followed within a few nanoseconds by diode current interruption.

Zusammenfassung

Das Anodenplasma in einer fremdmagnetisch isolierten Ionendiode

Ein Modell zur Beschreibung von Aufbau und zeitlicher Entwicklung des Anodenplasmas im Beschleunigungsspalt einer fremdmagnetisch isolierten Ionendiode wurde entwickelt. Wasserstofffreisetzung aus einem Ti-Pd Film und Ionisationsprozesse im Spalt werden in Modell berücksichtigt. Das Modell wird zur Analyse der quasineutralen Zone mit ihrem selbstkonsistenten elektrischen Feld und der Preanodenschicht mit elektrischem Potential von welcher der Ionenstrahl extrahiert wird, verwendet. Die Elektronendiffusion von der Kathode wird als turbulent angenommen. Damit stellt sich eine konstante Elektronendichte im Spalt ein. Die Untersuchungen wurden für verschiedene zeitabhängige Diodenspannungen mit Maximalspannung bis zu mehreren Megavolts und für Zeiten bis zu 100 ns durchgeführt. Für die Rechnungen wurden ein analytisches und ein 2 dim numerisches Modell verwendet. Im Verlauf des Diodenbetriebes kommt es zum vollständigen Abbau des Plasmas in der quasineutralen Zone und als Folge davon zum Zusammenbruch des Diodenstromes innerhalb weniger Nanosekunden.

CONTENT

1. INTRODUCTION

In applied-B ion diodes schematically shown in Fig. 1 ion beams are generated by acceleration of the ions in an electric field **E** applied across the anode-cathode gap[1]. The external magnetic field **B** applied parallel to the electrodes prevents a free propagation of electrons thus providing mainly an ion current. A theoretical modeling of different physical phenomena in the accelerating gap should accompany the design of the ion diodes. The different processes in the gap can be divided in those developing in the main volume of the gap and those occuring in a rather thin plasma layer near the anode from which the ions are extracted before the acceleration. Properties of the anode plasma, such as its non-homogeneity along the anode surface, its thickness and chemical content, are important for formation of an ion beam of small microdivergence. In this work mainly processes occuring in the thin anode plasma layer are analyzed. The discussed model covers also those processes occuring in the gap being necessary for a consistent theoretical description of the diode. Further implementation of additional mechanisms important for a realistic comparison of theoretical and experimental results will be done in a second step of the modeling.

Up to now no consistent model of the anode plasma including the plasma formation, the self-consistent discharge development and the mechanism of ion extraction from the anode plasma during the operation cycle is existing. Such a model would be useful for better understanding of the processes in the anode plasma of applied–B ion diodes.

In this report it is assumed that the anode plasma is produced by a perpendicular electric field **E** rising up for further acceleration of the ions across the gap between the anode plate and the virtual cathode. Such approach seems to be reasonable as an intermediate step on the way to a self-consistent numerical modeling of the ion diode in which the principal mechanisms of the anode plasma production are taken into account.

For investigation of the anode plasma during the operation cycle of 10^2 ns with gradual increase of the gap voltage φ_a from zero up to a maximal voltage φ_{max} both the development of the neutral gas layer and the dynamics of the breakdown in the applied magnetic field are important. In this work an analysis appropriate for such problems is done. As an example it is shown that at short delay times between the heating of the hydride film and the application of the perpendicular electric field the anode plasma layer exists only for some limited time of several tenths of nanoseconds. Then the operational cycle interrupts because of the exhaustion of the ion source. Thus the lower limit for the delay time is obtained. Numerical simulations of the ion diode start from an initially empty gap. Then during a few nanoseconds hydrogen gradually vaporizes from the anode due to the heating of the film. The process of the hydrogen release from the film is simulated using the simple model for hydrogen diffusion in solid material. The vaporization continues during all the operational cycle up to reaching φ_{max}.

The modeling is split into two parts. The first part contains a preliminary analysis based on analytical models in which a non-homogeneous gas layer of neutral atomic hydrogen is assumed beforehand. Anode plasma formation is discussed and the main equations for the anode plasma are derived. Then processes of electron diffusion and ionization in crossed **E** and **B** fields, structure of a pre-anode electrostatic sheath and development of a quasi-neutral layer are considered without accounting for the erosion of the anode plasma. This analysis is necessary for a

principal understanding of the interaction between the physical processes, which allows to simplify the numerical simulation of the anode plasma layer carried out afterwards. In the second part a detailed description of a code for a self-consistent calculation up to $\varphi_a = \varphi_{max}$ is given. First numerical calculations showed a physically reasonable development of the discharge both for the initial stage of the external electric field applied across the gap and for the second stage with prevailing role of the self-consistent field and of erosion effect. Results for calculated scenarios with φ_{max} = 1, 2 and 5 MV are presented. Despite the rather early stage of modeling the obtained characteristic plasma parameters are discussed in relation to the available experiments[2-5].

2. STATE OF THE ART IN ANODE PLASMA FORMATION AND MODELING

There are several ways for formation of anode plasma. For example, it can be produced by photon ionization of the background gas irradiated with a flash lamp[6]. Rather robust for production of the anode plasma are anode flashover discharges[7] and discharges in an additional electric field parallel to the anode[8]. In the flashover discharge the anode plasma is produced due to application of the accelerating voltage. Electrons available in the gap impact the anode plate and cause a breakdown in the gas desorbed from the anode surface after the impact. Because the accelerating voltage is a necessary condition for the anode plasma production, this is an example of 'passive' discharge. By applying an additional electric field near the anode surface an 'active' discharge is obtained. If assuming the possibility for a voltage drive at initial stage of the pulse, this traditional separation becomes rather conventional. A substantial shortcoming of the passive flashover discharge is the rather complicated chemical content of the anode plasma.

Since several years developments of active sliding discharges for production of the anode plasma are under way[9,10]. The sliding discharge develops at the anode plate made of a dielectric material after a breakdown in the parallel electric field, which also is directed parallel to the magnetic field. In order to improve the homogeneity of the anode plasma, the anode plate is covered by a thin titanium film of controlled thickness 500 Å, and Ti is protected from oxygenation by palladium film of thickness 200 Å. Beforehand this film structure is filled with hydrogen, which accumulates mainly in Ti. Initially the electric field produces a current in the hydride film thus heating it and then releasing hydrogen. With increasing gas density the breakdown condition near the anode is fulfilled and the sliding discharge develops creating the anode plasma. After this stage the accelerating electric field **E** is applied perpendicularly to the anode.

The physics of magnetically insulated ion diodes and of anode plasmas is described in Refs. 11 and 12. In Ref. 11 the investigations concerning the flashover anode plasma and in Ref. 12 also those for the sliding discharge plasma are reviewed comprehensively. Recently experimental investigations were carried out on anode plasmas produced by the sliding discharge[2] and on plasmas in the main volume of the gap[3]. The gap plasma is investigated in many details although there are remaining principally not solved problems. Good agreement between theory (the Desjarlais model[13]) and experimental observations is obtained during the most important stage of rising up the voltage. This phase of the diode operation is followed after about

10^2 ns by a breakdown between the anode and cathode electrodes. Attempts to develop numerical and analytical models for the gap breakdown are described in Refs. 14 and 15.

As to the modeling of the anode plasma, there are still many questions concerning its behavior and formation of such important parameters as the plasma density and temperature. For example the role of the self-consistent electric field, which remains in the anode plasma after development of the discharge, seems to be not investigated properly. One of the available theoretical analyses[5] addresses the flashover discharge. The electric field in the anode plasma was ignored. The density of the desorbed gas was not mentioned, perhaps because it was implicitly assumed to be rather small and comparable with the electron density of $2 \cdot 10^{15}$ cm^{-3}. This value is much less than the gas density in the sliding discharge with previously vaporized gas, which is about three orders of magnitude larger[9]. The analysis of Ref. 9, although addressing the sliding discharge, concentrates mainly on the development of avalanches in the pre-anode layer of the vaporized hydrogen thus predicting only a maximal value of the electric field. The electron density was obtained to be much less than that of the gas. Thus the anode plasma is rather weakly ionized.

Recently a 1 dim hydrodynamics model for the atomic hydrogen anode plasma was presented[16] including references describing details of the algorithms used in previously developed codes[17,18]. The investigation concerns mainly flashover discharges because the initial density is rather small and the anode plasma get to be fully ionized. The electric field is directed perpendicularly to the anode. It was assumed that initially near the anode exists either a hydrogen plasma or a neutral gas of hydrogen atoms of density 10^{16} cm^{-3} occupying homogeneously a pre-anode layer of 2 mm thickness. Calculations were carried out for only 4 ns having been started after the instantaneously applied maximal voltage across the gap $\varphi_{\max}$. In the modeling a gap size of 1.5 cm and an applied magnetic field B of 4 T were used. Results were given for $\varphi_{\max}$ = 5 MV and 10 MV. The erosion rate of the anode plasma was obtained. From the mentioned references it is not clear how the elementary kinetic processes in the applied magnetic field, which play a decisive role in the discharge, such as ionization, charge exchange and elastic and inelastic collisions, were modeled. Calculated values of the self-consistent electric field were not given.

The presence of the self-consistent electric field in the anode plasma can substantially influence the energetic spectra of the charged particles thus making necessary to account for the fields, e.g. in algorithms used for interpretation of spectroscopy measurements. Slowly oscillating or quasi-stationary electric fields, which are significantly perpendicular to the anode plate, had been measured in a flashover discharge plasma experimentally[11] but these fields rather arbitrarily were prescribed to instabilities developing inside the plasma. In this respect the problem may also concern the extraction of the ions from the edge of the plasma for further acceleration. The extraction occurs in electrostatic sheaths enveloping the anode plasma. The instabilities in the sheaths may also produce non-isotropic electric fields vanishing inside the anode plasma. Thus investigation of the extraction mechanism, which is coupled with the processes in the anode plasma, is also important.

This report presents only a very first step on this way. It is assumed that the anode plasma is produced due to the accelerating electric field **E** at an early stage of its rising up. Thus an intermediate conception of a passive discharge with a driving of the voltage is suggested. The analysis of a passive discharge is reasonable at the beginning of a consistent investigation concerning both the anode plasma and the

main volume of the accelerating gap. The rather direct mechanism of plasma production only by the perpendicular component of the electric field allows to analyze in detail principally important processes in the frame of a rather compact modeling. Moreover, as it is discussed in chapter 12, the active discharges may also transform into passive discharges due to a self-consistent transformation of the initially parallel electric field into the perpendicular field.

A simple model of the neutral gas production by an independent heating of the hydride film covering the anode is presented. In experiments rather contaminated plasmas are obtained but only the theoretical case of pure atomic hydrogen anode plasma is analyzed in this work. Thus the modeling of hydrogen diffusion through the protective film doesn't include the reaction $H + H \rightarrow H_2$ at the anode surface, which was considered in Ref. 9. Due to this simplification in diffusion equation the boundary condition at the anode surface is given as $n_{H|anode} = 0$ with n_H the hydrogen density in the film.

For the analysis of the anode plasma a rather moderate change of the applied magnetic field during the operation time is not principally important. Thus **B** in this work is assumed to be homogeneous across the gap and stationary. At least for the first stage of the diode operation before the gap breakdown this assumption is adequate. According to Ref. 3, during this stage B deviates from its average value of 3 T for not more than 30% what is quite sufficient for neglect in the simplified model. It is shown that in the anode plasma the self-consistent electric field is getting much less than in the main volume of the gap. Due to this the diamagnetic current of electrons becomes rather small thus resulting in a homogeneous magnetic field inside of the anode plasma. The current collapse[13], which occurs after gap breakdown, is not analyzed here. An adequate analysis for later stages seems to require not only to take into account the change of the magnetic field in the gap but also the implementation of some turbulent mechanisms for the gap plasma[14], this is out of the scope of this work.

It is assumed also that the values of B are not constrained by the critical magnetic field B_c as $B > B_c$. The critical field defines a margin of magnetic insulation against collisionless penetration of electrons through the gap after their starting from the cathode in crossed homogeneous **E** and **B** fields. In order to avoid this kind of gap breakdown it is assumed that near the cathode the electric field strength is always small due to development of a virtual cathode and the cathode electrons cannot freely increase their energy crossing the gap because of some mechanism of their cooling. The nature of the cooling is not discussed here, but this assumption agrees well with the experimental conclusions about rather small kinetic energies of electrons in the gap. For example according to Ref. 3, from the measurements of the dispersion coefficient in the gap plasma by an interferometer it was concluded that the plasma is rather cold. More experimental information on the temperature of the gap plasma is not available.

3. ZONE MODEL OF HYDROGEN DIFFUSION IN CRYSTALS

The problem to be considered here concerns the dynamics of the hydrogen release from a structure consisting of a film covered by a thin protective layer of thickness h_2 after fast heating from the initial temperature T_{min} to the final temperature T_{max} during the time t_h. This process is used for filling the pre-anode space with a

neutral gas needed for the plasma formation before applying high voltage to the anode-cathode gap. In Ref. 9 a Ti film covered by a Pd layer of $h_2 = 200$ Å, $T_{min} = 300$ K, $T_{max} = 1900$ K (melting temperature of Ti) and $t_h \approx 20$ ns is used. A rather simple zone model of hydrogen diffusion in the structure is considered below and the gas distribution in the pre-anode is calculated providing initial and boundary conditions at the anode for further consideration of the electric breakdown of the gas.

Particle energy states E of hydrogen atoms dissolved in a plane layer structure are schematically shown in Fig. 2. The parameters E_1 and E_2 define the energy levels of localized states in the layers, U_1 and U_2 define the bottom energies of the zone of free states of hydrogen atoms relative to the neighboring layers ($x > 0$ describes the empty space of the anode-cathode gap). The values of E_i and U_i ($i = 1, 2$) should be chosen to fit appropriately needed properties of real films.

The population density of the dissolved gas at the localized states is designated as n_{l1} and n_{l2}, the gas density of free states as n_{f1} and n_{f2}, the whole gas density as n_1 and n_2 ($n_i = n_{li} + n_{fi}$). The free population obeys a diffusion equation accounting for spatial changes of the potential energy of atoms, for excitations of atoms from localized states to free states and for reverse transitions from free states to localized states. The complete equation is given as

$$\frac{\partial n_{fi}}{\partial t} = \frac{\partial}{\partial x}\left(D_i \frac{\partial n_{fi}}{\partial x} + n_{fi}\mu_i \frac{\partial U}{\partial x} \right) + n_{li}\nu_{ei} - n_{fi}\nu_{di} \qquad (1)$$

with D_i the diffusion coefficient, μ_i the mobility of the free atoms in the internal potential field $U(x)$, ν_{ei} and ν_{di} the transition frequencies between localized and free states. The density of the localized states is described by the equation

$$\frac{\partial n_{li}}{\partial t} = -n_{li}\nu_{ei} + n_{fi}\nu_{di} \qquad (2)$$

The spatial change of $U(x)$ is shown in Fig. 2. The potential is constant inside each layer of the film but jumps near the layer boundaries. The Einstein relation is assumed for the coupling of the mobility and the diffusion coefficient: $D_i = \mu_i T$ with T the homogeneous temperature inside the film. For the diffusion coefficient the approximate expression $D_i = C_{Di} a_i \upsilon_T$ is used with a_i the crystal elementary cell size, υ_T characteristic velocity of free atoms given as $\upsilon_T = (2T/m_H)^{1/2}$. The realistic hydrogen mass m_H is used in the expression for υ_T because the effect of mass re-normalization of hydrogen quasi-particles is included into the fitting constant C_{Di} as well as the characteristic free path of the quasi-particles in the crystalline structure. The relation between the frequencies ν_{ei} and ν_{di} is chosen in the simplest way by assuming Local Thermodynamic Equilibrium (LTE). In this case the Boltzmann distribution is valid for the ratio of the localized and free population densities. Then the relation of the frequencies is given as $\nu_{ei}/\nu_{di} = (T/E_i)\exp(-E_i/T)$. The factor T/E_i accounts qualitatively for the statistical weight g_{li} and g_{fi} of the localized and the free states. The weights are assumed to be proportional to characteristic atomic energies: $g_{li} \propto E_i$, $g_{fi} \propto T$.

For ν_{di} it is assumed that its value is large enough to provide LTE at each position x of the structure. In this case the value of ν_{di} doesn't appear in the diffusion equation and thus is not important. The simplest estimation for ν_{di} is used according

to $\nu_{di} = (\upsilon_T/a_i)(m_H/m_i)$. Nevertheless this estimation accounts for the large difference of the hydrogen and crystals atomic masses (for Ti-Pd structure $m_1 = 46\, m_H$, $m_2 = 106\, m_a$, $a_1 \approx 3\cdot10^{-8}$ cm, $a_2 \approx 4\cdot10^{-8}$ cm). At $T = 1.9\cdot10^3$ K it is obtained $\upsilon_T = 5\cdot10^5$ cm/s, $\nu_{d1} \approx 4\cdot10^{11}$ s^{-1}, $\nu_{d2} \approx 10^{11}$ s^{-1}. From these estimations it follows that LTE is valid for the time intervals of both heating ($t_h = 2\cdot10^{-8}$ s) and diode operation ($t_{\max} = 5\cdot10^{-8}$ s).

After replacing the last two terms of Eq. (1) by the Left Hand Side (LHS) of Eq. (2) and then in case of LTE neglecting LHS in Eq. (2), Eq. (1) is transformed into

$$\frac{\partial n_i}{\partial t} = \frac{\partial}{\partial x} D_i \left(\frac{\partial}{\partial x} \left(\frac{n_i}{1 + (E_i/T)\exp(E_i/T)} \right) + \frac{n_i/T}{1 + (E_i/T)\exp(E_i/T)} \frac{\partial U}{\partial x} \right) \tag{3}$$

Defining then the new function

$$N_i = \frac{n_i \exp(U/T)}{1 + (E_i/T)\exp(E_i/T)} \tag{4}$$

Eq. (3) is transformed finally into the diffusion equation for N_i as

$$\frac{\partial}{\partial t} \left(\left(1 + \frac{E_i}{T} \exp\left(\frac{E_i}{T} \right) \right) \exp\left(-\frac{U}{T} \right) N_i \right) = \frac{\partial}{\partial x} \left(D_i \exp\left(-\frac{U}{T} \right) \frac{\partial N_i}{\partial x} \right) \tag{5}$$

Boundary conditions for Eq. (5) are defined as

$$\frac{\partial N_1}{\partial x} \to 0 \quad \text{at} \quad x \to -\infty, \qquad N_2 = 0 \quad \text{at} \quad x = 0 \tag{6}$$

The boundary condition at $x = 0$ is approximate. It is valid in case of small density of the neutral gas near the anode plate compared to the characteristic gas density in the transition layer (layer 2). This condition is always fulfilled because of the large difference of the diffusion velocity through the structure and the expansion velocity of the gas across the gap. Calculating the flux of hydrogen atoms through the anode surface on the base of Eq. (5) and Eq. (6), the distribution of neutral gas in the gap is obtained in the next chapters. There independent problem of the gas expansion is solved using obtained in this chapter time dependent number flux of the gas at $x = 0$.

The results of solution of Eq. (6) for the case of $E_1 = E_2 = U_1 = U_2 = 0.5$ eV, $C_{D1} = 4$, $C_{D2} = 3.8$, $T_{\min} = 300$ K, $T_{\max} = 1900$ K are shown in Fig. 3 and Fig. 4. Fig. 3 demonstrates that the change of the gas density in the storage layer (layer 1) is negligibly small. In the calculation the temperature rises up linearly reaching $T_{\max}$ at time 20 ns and then keeps constant. Due to this after 20 ns the evolution becomes quasi-stationary with the gas distribution in the transition layer being practically constant. Fig. 4 shows the time dependence of the hydrogen number flux from the anode plate. The flux reaches the value of $2\cdot10^{23}$ cm^{-2}s^{-1} during 20 ns and then keeps practically constant.

4. ANODE PLASMA FORMATION

At a given initial distribution of the neutral gas main features of the operation scenario can be qualitatively described in the following way. In the course of the voltage increase electron impact ionization of the neutral gas produces a quasi-neutral plasma layer which occupies the volume of the gas distribution near the anode (starting electrons can be provided anyhow and the reason of their appearance in the anode-cathode gap is not important). The plasma layer screens the anode from the cathode thus an electric potential drop arises mainly between the layer and the cathode. This layer plays the role of a virtual anode from which ions start to accelerate freely across the applied magnetic field. The voltage distribution is given in Fig. 5 as well as the densities of the neutral gas and the plasma components - ions and electrons.

Fig. 5 not only demonstrates the behavior of the main parameters but also shows some results of the calculations for maximal voltage increase $\Delta\varphi$ of 1 MV and a gas density n_g of 10^{17} cm^{-3}. The plasma is accumulated according to the thickness of the neutral gas distribution and is weakly ionized (the electron and ion densities n_e and n_i in the layer are two orders of magnitude smaller than n_g). Three regions are to be considered separately, the anode electrostatic sheath in which n_e and n_i are significantly different, the quasineutral plasma layer with $n_e \approx n_i$ and the main volume of the gap which is also an electrostatic sheath with different n_e and n_i adjusted to the cathode. The voltage changes mainly in the cathode sheath in which the ion beam is accelerated. But despite the small voltages the anode sheath and the quasineutral layer are necessary for the generation of the ion beam.

As it is shown in chapter 8, in the quasineutral layer ionization may increase the plasma density but don't contribute to the ion flux through the diode. The ion flux arises due to ionization in the anode electrostatic sheath where quasineutrality fails and electric charge separation becomes significant. The more general calculations of the second part of this report based on a numerical model (chapters 9 and 10) account also for the contribution in the quasineutral layer and for the contribution of the cathode sheath.

Principally important may be the rather thin anode sheath. Due to the large variation of the electric field and the maximal density of the neutral gas the ion production in the anode sheath may dominate. This could result in a destabilizing role for the ion current through the diode and it could induce field emission (desorption) of impurities from the anode plate. Therefore its proper consideration is necessary. Due to earlier exhaustion of the neutral gas in the sheath at a low density of the neutrals, it may get not attached to the anode during all the operation time t_{max}. In this case an ionization wave arises causing erosion of the quasineutral layer from the anode edge. At the wave front ionized atoms leave the anode sheath moving through the rest of the quasi-neutral layer to the cathode. As will be shown in the second part, at the cathode edge the erosion can dominate resulting in complete exhaustion of the anode plasma.

In the first part a preliminary case without accounting for the exhaustion of the anode plasma is analyzed using mainly analytical method. Pure atomic hydrogen is chosen as neutral gas. The anode plasma is assumed to weakly ionized. The main parameters of the applied-B ion diode are chosen for this case as follows:

Size of the gap between the anode and the virtual cathode	L	= 1 cm
Maximal time of the diode operation	t_{max}	= $5 \cdot 10^{-8}$ s
Thickness of the neutral gas near the anode	l	= 0.1 cm

Density of the neutral gas	$n_{g0} = 10^{17}$ cm^{-3}
Maximal voltage between the electrodes	$\varphi_{max} = 10^6$ V
Strength of applied magnetic field	$B = 3$ T
Maximal ion flux to the cathode	$j_{max}=2\cdot10^{21}$cm^{-2}s^{-1}

5. MAIN EQUATIONS DESCRIBING THE ANODE PLASMA AND QUALITATIVE ANALYSIS

Due to the rather strong magnetic field electron diffusion in the quasineutral layer towards the anode plate is rather weak, therefore a fluid dynamic description of electrons is useful (but it is shown below that it is not sufficient). The lifetime of an electron in the gap could exceed t_{max} thus the electron fluid is described by the non-stationary continuity equation for the electron density n_e:

$$\frac{\partial n_e}{\partial t} + \frac{\partial n_e \upsilon_e}{\partial x} = \nu_i n_e \tag{7}$$

with t the time, x the distance from the anode plate, υ_e the diffusion velocity of electrons to the anode across the magnetic field and ν_i the electron impact ionization frequency. For weakly ionized plasmas both υ_e and ν_i are given as function of the electric field strength E and they are directly proportional to the neutral gas density n_g. For short times t_{max} recombination is small, but an accurate calculation of the dependencies of $\upsilon_e(E)$ and $\nu_i(E)$ is important for an adequate description of the electron fluid. The calculation of $\upsilon_e(E)$ and $\nu_i(E)$ is a kinetic problem which is separated from the hydrodynamic problem of Eq. (7).

The lifetime of an ion that crosses the gap or the anode sheath is much shorter than t_{max}, hence the accelerated ions are treated as quasi-stationary. Ions are collisionless in the sheaths, their Larmor radius is much larger than the free path and the gap size. Collisionless ions are described by a kinetic equation. Its solution in the cathode sheath is given as:

$$n_i = \frac{j_0}{\sqrt{(2e/m_a)(\varphi_b - \varphi(x))}} + \int_{x_b}^{x} \frac{\nu_i(x')n_e(x')dx'}{\sqrt{(2e/m_a)(\varphi(x') - \varphi(x))}} \tag{8}$$

with m_a the ion mass, φ the electric potential ($E = -d\varphi/dx$), j_0 the ion flux incoming to the cathode sheath. The parameter x_b denotes conventional separation boundary between the cathode sheath and the quasineutral layer, φ_b the potential at the boundary. A similar equation is valid in the anode sheath (at this $x_b \to 0$, $\varphi_b \to \varphi_a$ with φ_a the anode potential, but $j_0 \to 0$ because no incoming flux from the anode plate is assumed).

The collisionless approximation for ions is not valid in the quasineutral layer. There the most important collision process is charge-exchange. For hydrogen its cross-section is $\sigma_{ex} \approx 5\cdot10^{-15}$ cm^2. The cross-section depends rather weakly on the ion velocity thus this dependence is neglected. The ion free path λ_i at the density of neutral gas $n_g \sim 10^{17}$ cm^{-3} is $\lambda_i \sim 1/n_g\sigma_{ex} = 2\cdot10^{-3}$ cm. Thus in the quasineutral layer of

thickness of $l = 0.1$ cm charge exchange processes dominate. Therefore in the layer ions are described by the fluid equation for the plasma density $n = n_i = n_e$ as:

$$\frac{\partial n}{\partial t} + \frac{\partial n v_i}{\partial x} = \nu_i n\,, \qquad v_i = \sqrt{e E \lambda_i / 2 m_a} \tag{9}$$

with v_i the mean ion velocity. Eq. (9) describes in simple way ions appearing after charge exchange or those produced by ionization and then accelerated in the electric field between collisions. Between the collisions the electric field is assumed to be locally homogeneous. After passing the distance λ_i ions transfer their positive charge to neutral atoms which start from zero velocity after ionization. The mean velocity of neutral atoms is negligibly small (see the Conclusions) and thus not calculated in this part.

The electric potential is described by the Poisson equation:

$$\frac{d^2\varphi}{dx^2} = 4\pi e\left(n_e + n_{ec} - n_i\right). \tag{10}$$

The density n_{ec} describes electrons appearing in the gap not due to ionization but after emission from the virtual cathode situated at $x = L$. The boundary condition for Eq. (10) at $x = 0$ is chosen as $\varphi(0) = \varphi_a$. The anode potential φ_a is given as rising up function of t. At the cathode it is valid $\varphi(L) = 0$. If considering the cathode sheath an additional boundary condition $E(L) = 0$ should be used at the virtual cathode in order to obtain n_{ec}. The density n_{ec} is assumed to be homogeneous due to an effective turbulent diffusion caused by a strong electric field in the gap outside the region of the anode plasma.

In the analysis carried out in the first part the problem is split into the following three sub-tasks.

1. Calculation of the distribution of electrons in crossed magnetic and electric fields for obtaining the diffusion velocity $v_e(E)$ and the ionization frequency $\nu_i(E)$ (chapter 6).
2. Analysis of the anode sheath for formulation of the boundary conditions at the anode edge of the quasi-neutral plasma including the value of the potential drop and the energy spectrum of ions which come from the sheath (chapter 7).
3. Calculation of the potential drop and the density distribution in the quasineutral anode plasma and estimations of ionization for the cathode sheath (chapter 8).

A comprehensive analysis of the cathode sheath has been done elsewhere[13,19]. There potential distributions in the gap and space charge limited Child-Langmuir number fluxes of ions j_{CL} (amplified by electrons coming from the virtual cathode) are analyzed. The potential drop across the anode plasma layer is much less than that across the cathode sheath. Therefore the ion flux j_i is practically determined by the values of φ_a and L and is equal to the Child-Langmuir flux given according to

$$j_i \approx j_{CL}\left(\varphi_a\right) = \frac{\pi}{8}\left(2e m_a\right)^{-1/2} \frac{\varphi_a^{3/2}}{L^2}. \tag{11}$$

With $L = 1$ cm and $\varphi_a = 10^6$ V it is obtained $j_{CL} = 2\cdot 10^{21}$ cm^{-2}s^{-1}.

The system of Eqs. (7) – Eq. (11) mathematically defines the problem to be solved. In the following a short review of the problem is given. In accordance with Eq. (11), the flux j_i is a given function of time because of a given time dependence of φ_a. As it will be shown in the next chapters, the thickness a of the anode sheath is rather small: $a << l$. In a thin sheath the time derivative term in Eq. (7) is neglected resulting in a quasi-stationary problem for the anode sheath (the same is valid for the cathode sheath). In the relatively thick quasineutral layer the spatial derivative term is neglected in Eq. (7) because of the small diffusion velocity of the electrons. Thus comparing Eqs. (7) and (9) at $n_e = n$ and $\upsilon_i >> \upsilon_e$ it is obtained that the flux $j_i(x) = n\upsilon_i$ is constant over the quasineutral layer: $j_i \approx j_0$. If the whole ion flux is produced in the anode sheath, then the density in the quasineutral layer is obtained from Eq. (9) as:

$$n \approx \frac{j_0}{\sqrt{e E \lambda_i / 2 m_a}} \tag{12}$$

Making time derivative of Eq. (12) and replacing $\partial n/\partial t$ at $n = n_e$ by the Right Hand Side (RHS) of Eq. (7) (in which the spatial derivative term is neglected), the equation for the electric field in the layer is obtained using Eq. (11) as:

$$\frac{1}{2E}\frac{\partial E}{\partial t} + \nu_i(E) = \frac{3}{2\varphi_a}\frac{d\varphi_a}{dt} \tag{13}$$

To demonstrate the character of the solution of Eq. (13) an exponential dependence of φ_a on the operation time $t_{\max}$ is assumed: $\varphi_a \propto \exp(t/t_{\max})$. In this case a stationary solution $E(x)$ exists. Assuming for simplicity for the ionization frequency a linear function of E: $\nu_i \propto n_g E$, the solution of Eq. (13) is obtained as $E \propto 1/n_g(x)$. Hence the electric field increases with decreasing gas density. At the edge of the gas distribution the electric field increases rapidly and the quasi-neutrality fails. Thus in the cathode sheath the Poisson equation has to be solved. A detailed analysis is given in chapters 6 to 8.

6. ELECTRON DIFFUSION AND IONIZATION IN CROSSED ELECTRIC AND MAGNETIC FIELDS

For calculation of the electron diffusion velocity $\upsilon_e(E)$ and the ionization frequency $\nu_i(E)$ the following assumptions are used: the magnetic field **B** is directed along the z-axis, the electric field **E** is directed along the x axis, the y-axis is perpendicular to both vectors, along the y- and z-axis translational symmetry is valid. The fields are homogeneous and stationary. The electron motion in crossed electric and magnetic fields is shown schematically in Fig. 6. The trajectory of collisionless electrons in a magnetic field is a circle. The presence of the electric field causes an **E**×**B** drift along the y-axis. The x-coordinate of an electron can only slightly deviate from the position x_c of the leading center. Collisions cause a shift of the electron trajectories in x-direction. Only the interaction of electrons with the neutral gas is taken into account because the ionization degree is assumed to be small. The gyration frequency ω_{Le} is assumed to be much larger than the characteristic frequency of

elastic and non-elastic electron scattering by the gas. The collisions are assumed to be instantaneous and isotropic.

The equation for the collisionless motion of electrons is given as[20]

$$m_e \frac{d\mathbf{v}}{dt} = -e\left(\mathbf{E} + \frac{1}{c}[\mathbf{vB}]\right) \tag{14}$$

The solution of Eq. (14) is well known as gyration in a frame moving along the y-axis with the velocity $v_D = cE/B$ of the **E**×**B** drift:

$$v_x = v_\perp \cos\theta\,, \quad v_y = v_\perp \sin\theta - v_D\,, \quad v_z = \text{const}\,, \quad x = x_c + \frac{v_\perp}{\omega_{Le}}\sin\theta \tag{15}$$

with $v_\perp$ the constant projection of the electron velocity onto the xy-plane in the moving frame, $\theta = \omega_{Le}t + \theta_0$ the angle of the gyration phase, $\omega_{Le} = eB/m_e c$ the electron Larmor frequency and x_c the x-coordinate of the leading center.

Ionization in crossed magnetic and electric fields is quite different from that in parallel fields. Electrons cannot directly accelerate along the electric field lines. They increase their kinetic energy in the electric field only in the course of relatively slow diffusion across the magnetic field due to elastic collisions with the atoms. Such electrical heating up to the ionization threshold energy is significantly hampered by a relatively small energy loss at elastic collisions and by non-elastic collisions with excitation of atoms. In principle the problem of the kinetic energy balance should include electron collisions with excited atoms, but in our simplified analysis all atoms are assumed to be in their ground state. Hence only three kinds of electron impact with neutral atoms are considered: elastic collisions, excitation, and ionization.

Elastic collisions with hydrogen atoms are described by the following approximate expression for the cross-section[21]:

$$\sigma_{el} = \frac{\sigma_{0el}}{1 + k_{el}\left(\varepsilon_k/\varepsilon_i\right)^2} \tag{16}$$

with $\sigma_{0el} = 4\cdot10^{-15}$ cm^2 the maximal cross-section at $\varepsilon_k = 0$, ε_i the ionization threshold energy with $\varepsilon_i = 13.6$ eV, ε_k the electron kinetic energy with $\varepsilon_k = m_e v^2/2$. The factor $1+k_{el}$ with $k_{el} = 8$ is a decreasing factor of the elastic collision cross-section at the kinetic energy equal to the ionization threshold energy.

Collisional excitation is described by the Van-Regemorter formula[22] as:

$$\sigma_{ex} = \sigma_{0ex} \sum_n f_n \left(\frac{\varepsilon_i}{\varepsilon_n}\right)^2 \frac{\gamma\left(\varepsilon_k/\varepsilon_n - 1\right)}{\varepsilon_k/\varepsilon_n} \tag{17}$$

with σ_{0ex} the characteristic cross-section with $\sigma_{0ex} = 1.3\cdot10^{-15}$ cm^2. The summation is over the excited energy levels of the atoms. f_n are the oscillator strengths and ε_n the excitation energies of the levels. The function γ is approximated analytically as

$$\gamma(u) = 0.01\left(-0.15 + 6.5u + 6.7u^2 - 0.85u^3\right) \qquad (\text{at } 0 < u < 6)$$

The terms of the sum in Eq. (4) vanish below the excitation thresholds: $\gamma = 0$ at $u < 0$. At $u > 6$ the function γ is approximated as $\gamma(u) = (\sqrt{3}/2\pi)\ln(1+u)$. The oscillator strengths and energy levels for excitations from the ground state (the Layman series) are given[23] as $(f_1,\varepsilon_1[\text{eV}]) = (0.416,10.2)$, $(f_2,\varepsilon_2) = (0.079,12.09)$, etc. Due to the fact that the oscillator strength of the transition $(0 \to 1)$ is much larger than other ones, only one level ($n = 1$) is implemented now.

The ionization cross-section is given by an approximation formula according to

$$\sigma_i = \sigma_{0i} \frac{\varepsilon_k/\varepsilon_i - 1}{\left(2 + \varepsilon_k/\varepsilon_i\right)^2} \quad (\text{at } \varepsilon_k > \varepsilon_i) \tag{18}$$

with σ_{0i} the characteristic cross-section with $\sigma_{0i} = 7 \cdot 10^{-16}$ cm^2. At $\varepsilon_k < \varepsilon_i$ the ionization cross-section is equal to zero. The maximum of function $\sigma_i(\varepsilon_k)$ occurs at $\varepsilon_k = 4\varepsilon_i \approx 54$ eV. At ionization collision the impacting electron losses amount ε_i of its kinetic energy for release of a secondary electron. It is assumed that the rest of kinetic energy is afterwards divided equally between both the electrons.

For an adequate calculation of the diffusion velocity, and the ionization frequency and the distribution function of electrons electron collisions are simulated by the Monte-Carlo method, i.e. by random tests for electron evolution with averaging of the results. The Uniform Random Generator (URG) is used. Initially an electron is starting having zero velocity, gyrating in crossed fields and is undergoing collisions from time to time. The cycle of calculation corresponds to a collision. At each collision the gyration phase θ is chosen as $\theta = 2\pi r$ with r the next URG value. The x–coordinate of the electron and its velocity vector at the collision as well as its kinetic energy is calculated using Eq. (15). The whole cross-section σ is calculated on the base of Eqs. (16) – (18) as $\sigma = \sigma_{el} + \sigma_{ex} + \sigma_i$. The time since the previous collision is given as

$$\tau_c = \frac{1}{n_g \upsilon \sigma} \tag{19}$$

with υ the velocity at the moment of the collision. The kinetic energy after the collision changed according to $-2\varepsilon_k m_e/m_a$ if the probability σ_{el}/σ gets large enough: $\sigma_{el}/\sigma > r_1$ with r_1 the next URG value. Otherwise the kinetic energy is changed as $(\varepsilon_k - \varepsilon_i)/2$ if $\sigma_i/\sigma > (1 - r_1)$, otherwise as $\varepsilon_k - \varepsilon_{ex}$ (in the modeling $\varepsilon_{ex} = \varepsilon_1$ is used). The random vector of the electron velocity after the collision is calculated as

$$\upsilon_x = \upsilon\sqrt{1 - r_a^2}\cos 2\pi r_p, \quad \upsilon_y = \upsilon\sqrt{1 - r_a^2}\sin 2\pi r_p, \quad \upsilon_z = \upsilon r_a \tag{20}$$

with r_a and r_p the next URG values. Then the new position of the leading center is calculated using Eq. (15) and this cycle is repeated until fluctuations of the results become negligibly small (practically it is enough to simulate about a million collision cycles). Counters for the ionization collisions N, for the final position x_c of the leading center and for the collision times t give then the averaged diffusion velocity and ionization frequency as

$$\upsilon_e = \frac{x_c}{t}, \qquad \nu_i = \frac{N}{t} \tag{21}$$

For the calculation of the energy distribution function $F_e(\varepsilon_k)$ it is assumed that during the interval τ_c given by Eq. (19) the electron has the kinetic energy of the next collision moment. This assumption would give exact result for F_e at the limit of infinitely long calculation. The function $F_e(\varepsilon_k)$ is given as a table with values in some definite energy intervals $\varepsilon_j < \varepsilon_k < \varepsilon_{j+1}$ with j the index of the intervals $\Delta\varepsilon_j = \varepsilon_{j+1} - \varepsilon_j$. Each table value F_j is collected as the sum of times τ_c for which the kinetic energy belongs to the interval $\Delta\varepsilon_j$. Finally the distribution function is normalized per one electron, i.e. F_j obeys the condition

$$\sum_j F_j \Delta\varepsilon_j = 1 \tag{22}$$

From Eq. (19) follows that τ_c is reversely proportional to n_g. The same is valid for the time collector t. Thus if running up to a given number of ionization collisions N then $\nu_i \propto n_g$ in accordance with Eq. (21). The change of the leading center at collisions doesn't depend on n_g (it depends only on the value of the magnetic field and on the kinetic energy of the electron), the same is valid for the final position x_c. Therefore it is valid $\upsilon_e \propto n_g$ in accordance with Eq. (20). Thus there is a scaling law for n_g due to which it is sufficient to calculate ν_i and υ_e for only one neutral gas density. The distribution function $F(\varepsilon)$ after normalization doesn't depend on n_g.

Another scaling law concerns the magnetic field strength B. The symbol B appears only in the electric drift velocity $\upsilon_D = cE/B$ and in the electron Larmor radius $r_{Le} = \upsilon_\perp/\omega_{Le} \propto 1/B$. Thus the electric field strength E appears only in Eq. (15) together with B. Hence in order to keep the same values of electron kinetic energy and the same evolution in the velocity space at a change of B it should be changed also E proportionally to B. Electron shifts in the collisions are proportional to the Larmor radius, thus the final position of the leading center x_c changes reversely proportional to B. As a result it is obtained:

$$\nu_i = n_g \chi_\nu\left(E/B\right), \quad \upsilon_e = \frac{n_g}{B}\chi_\mu\left(E/B\right), \quad F_e = \chi_F\left(\varepsilon_k, E/B\right) \tag{23}$$

It is sufficient to calculate the functions χ_ν, χ_μ, χ_F at some B as functions of E and ε_k only and then to use these functions for arbitrary B.

Results of calculations at $n_g = 10^{17}$ cm^{-3} and $B = 3$ T are shown at Figs. 7 – 9 for the functions $\nu_i(E)$, $\upsilon_e(E)$, $\varepsilon_{\text{mid}}(E)$ with $\varepsilon_{\text{mid}} = \int \varepsilon F_e(\varepsilon) d\varepsilon$ the mean kinetic energy of the electron. The distribution function F_e is shown in Fig. 10 for different electric field strengths E. Table 1 demonstrates the distribution of energy loss of electron for elastic and non-elastic collisions at $B = 3$ T.

7. ANODE ELECTROSTATIC SHEATH

As will be shown below, the anode sheath is rather thin, hence if neglecting the neutral gas exhaustion a quasi-stationary approximation of Eq. (7) can be applied as

$$\frac{d n_e \upsilon_e}{dx} = \nu_i n_e \tag{24}$$

This results in the solution n_e obtained as:

$$n_e = \frac{j_0}{|\upsilon_e|}\exp\bigl(-\xi(x)\bigr), \qquad \xi(x) = \int_0^x \frac{\nu_i(x')}{|\upsilon_e(x')|}dx' \tag{25}$$

If neglecting the electron flux from the quasineutral layer, the electron flux towards the anode at $x = 0$ is equal to the backward ion flux j_0 at the boundary between the anode sheath and the quasineutral plasma layer of thickness l. In the analysis of the quasi-stationary problem the flux j_0 is considered as a given constant parameter. As it follows from Eq. (23), the relation ν_i/υ_e under the integral of Eq. (25) doesn't depend on n_g. This function has a maximum value equal to 750 cm^{-1}. Because at constant B it depends on x only via E. After normalization on the maximum this function is designated as $k(E)$ and is shown at Fig. 11 for $B = 3$ T . In the anode sheath the values of E are rather large, thus in accordance with Eq. (25) it is valid $\xi \sim 1$ at $x = a = 1/750 = 1.3\cdot10^{-3}$ cm. The parameter a with $a \propto 1/B$ is used as the characteristic sheath thickness. Since $a << l$, the investigation of the anode sheath for the limit $a/l \to 0$ is completed. In this limit charge-exchange collisions in the sheath are neglected.

The ions are described by Eq. (8) and the electric potential by Eq. (10) neglecting the small contribution of the cathode electrons ($n_{ec} = 0$). The boundary condition for Eq. (10) at $x = 0$ is given as $\varphi(0) = \varphi_a$ with φ_a the anode potential. If $a/l \to 0$, another boundary condition is given as $\varphi(x) \to \varphi_a - \Delta\varphi_a$ at $x \to \infty$ on an infinitely small scale of the anode sheath with $\Delta\varphi_a$ the still unknown potential drop over the sheath. Thus the equation for φ becomes

$$\frac{d^2\varphi}{dx^2} = 4\pi e j_0\left(\frac{\exp\bigl(-\xi(x)\bigr)}{|\upsilon_e(x)|} - \int_0^x \frac{\exp\bigl(-\xi(x')\bigr)d\xi(x')}{\sqrt{(2e/m_a)\bigl(\varphi(x')-\varphi(x)\bigr)}}\right) \tag{26}$$

The value of $\Delta\varphi_a$ is obtained from the requirement of smooth transition of the solution of Eq. (26) to the solution of the quasineutrality equation $n_e = n_i$. The quasineutrality equation at $x \to \infty$ is obtained requiring in Eq. (26) the RHS to be zero. For a rather small electric field E ($E < 10^5$ V/cm) a linear fitting for $|\upsilon_e|$ is used: $|\upsilon_e| \approx \mu E$ with $\mu = 50$ cm^2/s/V for $n_g = 10^{17}$ cm^{-3} and $B = 3$ T. It is valid $\mu \propto n_g/B^2$ at a constant E/B.

To solve the problem of Eq. (26) it is convenient to use ξ as a new coordinate instead of x and the function u defined below in Eq. (29) instead of φ. The ion flux j_0 is expressed via the maximal Child-Langmuir flux $j_{CL}(\varphi_{\max})$ given by Eq. (11) as $j_0 = \Gamma_0 j_{CL}(\varphi_{\max})$. Thus Eq. (26) is transformed as:

$$k\frac{d}{d\xi}\left(k\frac{du}{d\xi}\right)=\eta\left(q(\xi)-\frac{\exp(-\xi)}{g\,k du/d\xi}\right),\quad u(0)=0,\qquad u(\infty)=u_\infty \tag{27}$$

with the parameters η, u, q, k and g given as:

$$\eta=\frac{\pi^2}{4}\Gamma_0\left(\frac{\varphi_{\max}}{\varphi^*}\right)^{3/2}\left(\frac{a}{L}\right)^2 \tag{28}$$

$$u=\frac{(\varphi_a-\varphi)}{\varphi^*},\qquad \varphi^*=\frac{2e\,a^2}{m_a\mu^2} \tag{29}$$

$$q(\xi)=\int_0^\xi\frac{\exp(-\xi')d\xi'}{\sqrt{u(\xi)-u(\xi')}},\qquad x=a\int_0^\xi\frac{d\xi'}{k(\xi')} \tag{30}$$

$$k=aK\left(E^*k\frac{du}{d\xi}\right),\qquad g=g\left(E^*k\frac{du}{d\xi}\right)=\frac{|\upsilon_e|}{\mu E},\qquad E^*=\varphi^*/a \tag{31}$$

The function q depends not only on ξ but also on the behavior of $u(\xi')$ for all $\xi'<\xi$. u_∞ should be found from the requirement of zero RHS of Eq. (27).

For $a = 1.3\ 10^{-3}$ cm and $\mu = 1.5\cdot10^4$ in CGS units it is obtained $\varphi^* = 1.3\cdot10^3$ V. It is obtained also that $\varphi^* \propto (B/n_g)^2$. From Eq. (28) follows a limitation of parameter η. For example for $\varphi_{\max} = 10^6$ V, $L = 1$ cm and if $\Gamma_0 < 1$ it is obtained $\eta < 0.1$. At other conditions, e.g. at larger $\varphi_{\max}$, η may get much larger.

From Eq. (31) it is concluded that the function $k(du/dx)$ is a solution of an algebraic equation. The function g accounts for deviations from the fitting function $|\upsilon_e| \approx \mu E$. The function g is shown in Fig. 11 together with k. The electric field strength $E^* = 10^6$ V/cm. It is valid $E^*/B \propto (B/n_g)^2$ thus the range of the argument E in Fig. 11 is sufficient if n_g and B are limited as $B^{3/2}/n_g \le 5\cdot10^{-11}$ in CGS units. For others n_g and B the range has to be expanded by additional tabulation.

The solution of Eq. (27) is estimated for $k = g = 1$ in the following way. At small ξ the ion contribution $q(\xi)$ at the RHS of Eq. (27) can be neglected. Thus a simplest approximate solution is obtained as:

$$u \approx \alpha_0\xi - \tfrac{1}{2}\eta\xi^2/\alpha_0 + \ldots \qquad (\xi << 1) \tag{32}$$

The constant α_0 is given as $\alpha_0 = du(0)/d\xi$. Then the ion contribution is obtained as

$$q(\xi) \approx 2\sqrt{\xi/\alpha_0} \qquad (\xi << 1) \tag{33}$$

At $\eta >> 1$ the transition to the quasineutrality region occurs at $\xi << 1$. To fit the regions of the Poisson and quasineutrality solutions together at some point $\xi = \xi_1$ the ion and electron densities there as well as their derivatives should be of the same order. Thus, according to Eq. (27), it is valid $dq/d\xi \sim -(du/d\xi)^{-2}d^2u/d\xi^2$ and

$q \sim (du/d\xi)^{-1}$. Using Eq. (32) and Eq. (33) for the estimation at the point ξ_1, the equations for ξ_1 and α_0 are obtained as

$$\sqrt{\frac{\xi_1}{\alpha_0}} \sim \frac{1}{\alpha_0}, \qquad \frac{1}{\sqrt{\xi_1 \alpha_0}} \sim \frac{\eta}{\alpha_0^3} \tag{34}$$

From Eq. (34) it is obtained $\alpha_0 \sim \eta^{1/3}$, $\xi_1 \sim 1/\eta^{1/3}$ and $u(\xi_1) \sim 1$. Thus the initial condition for the quasineutrality equation $du/d\xi = q^{-1}\exp(-\xi)$, which is valid at $\xi > \xi_1$, is established as $u(1/\eta^{1/3}) \sim 1$. Using the dependence $u = u(\xi_1) + \alpha_0\xi$ for the estimation of $q(\xi)$ at $\xi < 1$, it is obtained $du/d\xi \sim (\eta^{1/6}/\xi^{1/2})\exp(-\xi)$. Integration of this estimation equation results in $u_\infty \sim \eta^{1/6}$. Hence at $\eta >> 1$ the value of u_∞ is formed mainly in the quasineutral region.

Now it will be shown that at $\eta << 1$ it is valid $\xi_1 >> 1$ and the value of u_∞ is formed mainly in the Poisson region. After neglecting q, a solution $u(\xi)$ of the Poisson equation with $du/d\xi$ vanishing at large ξ is obtained at $1 << \xi << \xi_1$ as

$$u = 2\sqrt{2\eta}\left(1 - \exp\left(-\xi/2\right)\right) \tag{35}$$

The calculation of $q(\xi)$ with this $u(\xi)$ after neglecting a small contribution of $\exp(-\xi/2)$ under the square root in the integral of Eq. (30) gives $q \sim 1/\eta^{1/4}$. Because it is valid $q(\xi_1) \sim (du/d\xi)^{-1}\exp(-\xi_1)$ with u given by Eq. (12), it is obtained $\xi_1 \approx \ln(1/\sqrt{\eta}) >> 1$. The logarithm here is really of the order of one, i.e. it is valid $\xi_1 > 1$. Nevertheless in the estimation the inequality $\xi_1 >> 1$ is used. Then from the integration of the quasineutrality equation $du/d\xi = \exp(-\xi)/q$ for $\xi_1 < \xi < \infty$ the increment of u is obtained as $u_\infty - u(\xi_1) \sim \eta^{3/4}$. This is much less than the result of Eq. (35) at $\xi = \xi_1$. Hence in accordance with Eq. (35) it is obtained $u_\infty \approx 2^{3/2}\eta^{1/2}$ at $\eta << 1$.

This estimation demonstrates the existence and the principal physical features of a solution describing the transition from the Poisson region with a strong electric field to the quasineutral region with zero electric field. To obtain the numerical solution it is necessary to account for the behavior of the function k and g. Since $k \to 0$ at small E, it is impossible to obtain formally a physically reasonable stationary solution at $x \to \infty$. But the real problem is a non-stationary one. Due to this at some finite x the term $\partial n_e/\partial t$ of Eq. (7) becomes larger than $\partial(n_e v_e)/\partial x$ thus making the consideration of exact limit $E \to 0$ senseless. In order to keep the physical picture of a smooth transition from the narrow sheath to a wide quasineutral layer a limitation of k from below at small E is applied in the calculation ($k > k_0$). Due to a rather weak influence of k_0 for u_∞ the appropriate artificial value $k_0 = 0.2$ is chosen.

From Eq. (8) follows the expression for the energy distribution function $f_i(\varepsilon)$ of ions leaving the anode sheath as $f_i(\varepsilon) = (e^{-1}E^{-1}(x)dn_i/dx)|_{x:\{e\varphi(x)=\varepsilon\}}$ with ε the ion kinetic energy.

The values of $\Delta\varphi_a = \varphi^* u_\infty$ for a possible range of η are shown in Fig. 12 as results of the calculation using the function g and the corrected function k of the Fig. 11. The electric field strength E for each η is maximal at the anode. This maximum E_a increases as η increases and is equal to the maximal table value $E_a = 10^6$ V/cm at $\eta = 0.046$. For this reason larger values of η are not considered. The

values of η in the calculations are much less than in the estimation because typically the values of k are significantly less than those used in the estimation. The mean energy $\varepsilon_{i\mathrm{mid}}$ of ions leaving the sheath for further propagation in the quasi-neutral anode plasma layer is defined as $\varepsilon_{i\mathrm{mid}} = \int \varepsilon f_i d\varepsilon / n_i$. $\varepsilon_{i\mathrm{mid}}$ is also shown in Fig. 12. The mean ion energy is significantly less than the potential drop over the sheath determined by the behavior of f_i.

The sheath thickness is defined as the distance to the anode corresponding to $E/E_a = 0.1$. The dependence of the thickness on η is shown at Fig. 13. It increases significantly at rather small values of η. The thickness is much less than l hence the smallness of the sheath compared to the anode plasma layer is confirmed. The calculated behavior of the electric field and the densities of ions and electrons across the sheath are shown in Fig. 14. In this calculation the anode electric field is equal to 320 kV/cm. The energy distribution function of ions at the boundary between the sheath and the quasineutral layer is shown in Fig. 15 for $\eta = 0.028$. The maximum of the distribution function at the ion energy of about 60 eV corresponds to the maximum of the ionization cross-section and thus to the region of most effective ionization in the sheath with $E \approx 80$ keV/cm according to Fig. 7.

8. QUASINEUTRAL LAYER OF THE ANODE PLASMA

In the quasi-neutral layer the collisionless approximation for ions is no longer valid. The most important ion collision process is charge-exchange schematically shown in Fig. 16. Estimating the ion free path at a density of 10^{17} cm^{-3} of the neutral gas it is obtained, that even for the sheath in principle the collisions are becoming substantial. Hence in the quasineutral layer the charge exchange dominates. Therefore in this layer ions are described by a fluid equation with υ_i mean ion velocity. Such a model describes ions exchanging the neutral atoms after coming from the anode sheath or those produced by ionization and then in both cases accelerated in the electric field until the next collision. After passing the distance λ_{ex} ions transfer their positive charge to neutral atoms and then new ions accelerate starting from a negligibly small velocity.

The ion current after leaving the anode sheath penetrates through the quasineutral layer of the anode plasma. The thickness l of the layer is rather large compared to the thickness a of the anode sheath ($l >> a$). For this reason at the analysis of the layer the thickness of the anode sheath is neglected. Thus in the modeling it is assumed that the ions enter the layer at the anode position $x = 0$. From another hand, the layer thickness is much less than the gap size: $l << L$. Due to this smallness the analysis of the layer is completed adequately for $l/L \to 0$. The charge-exchange collisions in the layer change the ion energy distribution function significantly compared to the distribution of the entering ions. This change happens in a 'pre-sheath' of the thickness λ_i between the anode sheath and the layer. The pre-sheath is not analyzed in this work because the drop of electric potential over it is small compared to the potential drop over the anode sheath and over the quasineutral layer.

In chapter 5 it was mentioned that the ion flux is constant over the quasineutral layer. Due to this and using Eq. (9) the plasma density n in the layer is obtained as

$$n(x) = j_0 \sqrt{2 m_a \sigma_{ex} n_g(x) / e E(x)} \tag{36}$$

with j_0 the incoming ion flux. In Eq. (36) dependence on t is also assumed.

As was shown in chapter 7, the quasi-stationary ionization vanishes across the anode sheath as a result of transition to the rather thick quasineutral layer. Formally this is a consequence of neglecting the term $\partial n_e/\partial t$ in Eq. (7). In the quasineutral layer the term $\partial(n_e \upsilon_e)/\partial x$ of Eq. (7) is neglected. The ionization doesn't vanish only due to the term $\partial n_e/\partial t$. Therefore Eq. (7) transforms as:

$$\frac{\partial n}{\partial t} = \nu_i n \tag{37}$$

The initial condition for Eq. (37) is given as $n(x) \to 0$ at $t \to -\infty$.

As was shown qualitatively in chapter 5, a rather simple solution is possible if the voltage φ_a increases exponentially. If j_0 is increasing exponentially, a simple solution of Eq. (36) and Eq. (37) is possible as well. Such kind of scenario with $j_0(t) = j_{CL}(\varphi_{\max})\exp(3t/2t_{\max})$ providing appropriate understanding of the anode plasma behavior is considered in this chapter. In addition the spatial dependence $n_g(x) = n_{g0}\exp(-x^2/l^2)$ is assumed with l the thickness parameter of the layer. The time dependence of j_0 induces exponential increase of the plasma density, but the electric field strength in the layer is obtained to keep constant. Thus it is valid:

$$n \propto \exp\left(3t/2t_{\max}\right), \qquad E = E(x) \tag{38}$$

For the further analysis a convenient set of dimensionless variables is used as:

$$w = \frac{l}{\varphi^*} E, \qquad \xi = \frac{x}{l}, \qquad \rho = \frac{n}{n^*} \exp\left(-\frac{3t}{2t_{\max}}\right) \tag{39}$$

The potential φ^* is defined by Eq. (29). The density n^* is defined as

$$n^* = j_{CL}(\varphi_{a\max}) \sqrt{2 m_a l \sigma_{ex} n_{g0} / e \varphi^*} \tag{40}$$

At $\varphi_{\max} = 10^6$ V, $\varphi^* = 1.3 \cdot 10^3$ V, $l = 0.1$ cm, $\sigma_{ex} = 5 \cdot 10^{-15}$ cm^2 and $n_{g0} = 10^{17}$ cm^{-3} the value of n^* is obtained as $n^* \approx 5 \cdot 10^{14}$ cm^{-3}. In accordance with Eq. (28), the time dependence of the parameter η at these values of $\varphi_{\max}$ and φ^*, at the anode sheath thickness parameter $a = 1.3 \cdot 10^{-3}$ cm and at the gap size $L = 1$ cm is obtained as $\eta \approx 0.1\Gamma_0$ with $\Gamma_0 = \exp(3t/2t_{\max})$. The given function $\Gamma_0(t)$ determines the evolution of the anode sheath completely. Using the new variables Eqs. (1) and (2) are transformed as:

$$\rho(\xi) = \sqrt{g(\xi)/w(\xi)} \tag{41}$$

$$g(\xi)\overline{\nu_i}(w) = \alpha \tag{42}$$

with $g(\xi) = n_g(\xi)/n_{g0}$ the normalized density of the neutral gas, $\overline{\nu}_i = \nu_i/\nu_{\max}$ the ionization frequency normalized at $n_g = n_{g0}$, $\nu_{\max}$ the maximal ionization frequency (see the Fig. 7), $\alpha = 3/(2\nu_{\max}t_{\max})$ a dimensionless parameter. At $t_{\max} = 5\cdot10^{-8}$ s and $\nu_{\max} = 2.5\cdot10^{9}$ s^{-1} it is obtained $\alpha \approx 10^{-2}$.

For $\alpha << 1$ there are existing two formal solutions w of Eq. (42) corresponding to the non-monotonic behavior of the ionization frequency. Only the solution of a smaller value of w is physically reasonable in accordance with a decrease of the electric field strength at $\alpha \to 0$. This branch of the reversed function $\Lambda = \overline{\nu}_i^{-1}$ is shown at Fig. 17. Hence the dimensionless electric field strength is obtained as

$$w \approx \Lambda\left(\alpha / g\left(\xi\right)\right) \tag{43}$$

As an example, the corresponding electric field strength $E = (\varphi^*/l)w$, the potential drop $\Delta\varphi(x)$ in the layer and the plasma density $n = n^*\rho\exp(3t/2t_{\max})$ obtained for the mentioned scenario on the base of Eq. (41) and Eq. (43) are shown in Figs. 18 - 20. The potential drop is given as

$$\Delta\varphi = \varphi_0 - \varphi(x) = \varphi^* \int_0^{x/l} w\left(\xi\right) d\xi \tag{44}$$

The derivative of E in Fig. 18 tends to infinity at the right edge of $\xi = \xi_m$ of the quasineutral layer. Near this edge the term dE/dx is becoming comparable with the term $4\pi e n_i$ of Eq. (10). Estimating Eq. (43) near $\xi = \xi_m$ with the sign '–' at $\xi < \xi_m$ it is obtained

$$w\left(\xi\right) \approx 7 - 0.1\sqrt{1 - 10^{-2}\exp\left(\xi^2\right)} \tag{45}$$

The size Δx of the right charge separation region is obtained from the criterion $(\varphi^*/l^2)dw/d\xi = 4\pi e n^* \rho$ as $\Delta x \sim 10^{-3}$ cm. Thus the charge separation near the singularity at $\xi = \xi_m$ is negligible.

Qualitative profiles of voltage and density distributions are shown in Fig. 5 at $\varphi_{\max} = 1$ MV for the exponential increase of the anode potential. In the analytical model the ion flux to the cathode is equal to the electron flux to the anode. At $\varphi_{\max} = 1$ MV the maximal ion flux is obtained as $j_{\max} = 2\cdot10^{21}$ cm^{-2}s^{-1}. For $t_{\max} = 5\cdot10^{-8}$ s the number of ions reaching the cathode is estimated as $J_{\max} = 10^{14}$ cm^{-2}. The exhaustion of the neutral gas in the anode sheath is estimated by the factor $\iota = J_{\max}/an_{g0}$ with a the anode sheath thickness, n_{g0} the initial neutral gas density near the anode. In accordance with Fig. 13 for $a = 3\cdot10^{-3}$ cm and $n_{g0} = 10^{17}$ cm^{-3} it is obtained $\iota = 1/3$. Hence for the mentioned scenario the exhaustion of neutrals is almost reached.

The quasineutral solution formally continues at $\xi > \xi_m$ where for calculation of the ionization the right wing of the function $\nu_i(E)$ should be used. In reality it is unstable and thus not realizes at all. As it will be shown numerically, the cathode edge of the quasineutral layer is the additional source of ions accelerated in the gap due to erosion of the edge. The erosion is caused by the strong electric field in the gap separating electrons and ions at the edge. The separated electrons penetrate the

quasineutral layer diffusing towards the anode. If the erosion is significant, the simplified approach is not sufficient quantitatively but always remains useful for qualitative interpretation of the physical processes in the anode plasma. In the cases with the edge erosion the production of ions in the anode sheath decreases thus the exhaustion of neutrals there may become not substantial.

The ionization production of the ion flux in the cathode sheath and thus the erosion is negligibly small in case of the small density of the neutral gas and small rate of the ionization at the right wing of $\nu_i(E)$. If the ionization rate at $\xi > \xi_m$ would keep at its maximum, the contribution to the ion flux is estimated as

$$\Delta j_i = \int_{l\xi_m}^{\infty} \nu_i n_e \, dx < \nu_{\max} n^* l \int_{\xi_m}^{\infty} e^{-\xi^2} \sqrt{\tfrac{1}{7} e^{-\xi^2}} \, d\xi \qquad (46)$$

This contribution doesn't exceed $2 \cdot 10^{20}$ cm^{-2}s^{-1}, which is much less than the maximal Child-Langmuir flux $j_{CL}(\varphi_{\max}) = 2 \cdot 10^{21}$ cm^{-2}s^{-1}. A correction δj_i of the ion flux j_i caused by the term $\partial(\upsilon_e n)/\partial x$, which is omitted in Eq. (37), is obtained to be rather small for the considered scenario: $\delta j_i / j_i \sim 0.1$. Hence in this case the ion flux is produced mainly in the anode sheath.

To find the neutral gas velocity υ_g the work A of the electric field for the gas acceleration is estimated on the base of Fig. 19 at $\Delta\varphi = 500$ V as $A = e j_0(t_{\max}) \Delta\varphi t_{\max} \approx 10^5$ erg/cm^2. Thus from the energy balance $m_a l n_g (\upsilon_g)^2/2 = A$ it is obtained $\upsilon_g \approx 3 \cdot 10^6$ cm/s, thus resulting in a displacement of the gas distribution by the distance $\upsilon_g t_{\max} = 0.15$ cm.

9. NUMERICAL MODELING OF AN APPLIED-B ION DIODE

From the above analysis follows that both the anode sheath and the quasineutral layer seem to be important subjects for more detailed theoretical investigations at larger voltages ($\varphi_{\max} > 1$ MV). Further increase of the voltage or analysis for scenarios in which the density of neutrals at the cathode edge of the quasineutral layer are not small require take into account such phenomena as the edge erosion, the exhaustion of neutrals and motion of the neutral gas. This may open new interesting features of the anode plasma behavior. For many cases the analytical approach presented in the previous chapters cannot describe the physical processes in the diode and its operation scenarios properly. In order to be able to simulate numerically the characteristic features of the diode operation a 2 dim code for x- and υ- coordinates was developed. A description of this code as well as the results of the calculations are given below. The following problems are treated numerically:

Dynamics of the neutral gas with evaporation from the anode, ionization and acceleration due to the charge-exchange processes.

Dynamics of ions taking into account acceleration by the electric field and the charge-exchange deceleration.

Dynamics of electrons with diffusion in crossed E and B fields.

Electric field with solving the Poisson equation.

Of special concern is the 2 dim grid (x, υ_x). It has to fit the following regions:

x- coordinate: the anode sheaths (10^{-4} – 10^{-3} cm)

quasineutral layer (10^{-2} – 10^{-1} cm)

the whole gap (~ 1 cm)

υ - coordinate: the neutral gas velocities (0.1 – 100 eV)

the anode plasma ions (0.1 – 10^4 eV)

the accelerated ions (10^3 – 10^7 eV)

The x coordinate corresponds to the spatial coordinate across the anode-cathode gap with $x = 0$ at the anode surface and $x = L$ at the cathode. The velocity coordinate υ describes ions or neutrals. Only the most important x-component of the velocities of these particles is taken into account. Thus ions and neutrals are described using the Boltzmann equation with the collision term taking into account only most principal charge-exchange process. As to electrons, the hydrodynamics approach developed in the previous chapters is applied. The electric field E is directed perpendicularly to the electrodes and changes in space and time. The applied magnetic field is assumed to be strong enough for neglecting changes of B caused by the diamagnetic effect.

The details of the calculation are discussed in the following chapters: main equations of the problem are considered in chapter 9.1, the description of the features of the code is given in chapter 9.2, the results of the calculation are presented in chapter 10.

9.1. MATHEMATICAL PROBLEM

The model of hydrogen diffusion through the thin Ti–Pd structure describing the release of neutral gas from the anode surface into the gap is represented in chapter 3. According to this model, for establishing adequate boundary conditions at the anode the neutral gas flux at $x = 0$ is approximated as

$$j_g(0) = \frac{1}{2}\left(1 - \cos\left(\pi t / t_{g\max}\right)\right) j_{g\max} \text{ at } t < t_{g\max} \text{ and } j_g(0) = j_{g\max} \text{ at } t \geq t_{g\max} \quad (47)$$

In this work maximal gas flux $j_{g\max} = 2 \cdot 10^{23}$ cm^{-2}s^{-1} and the time of the flux increase $t_{g\max} = 20$ ns are given constants. The released atoms are assumed to have a Maxwell distribution function according to

$$f_g(0, \upsilon) = \frac{m_p}{T_a} j_g(0) \exp\left(-\frac{m_p \upsilon^2}{2T_a}\right) \text{ at } \upsilon > 0 \quad (48)$$

with m_p the proton mass, T_a the anode surface temperature assumed to be a linear function of time at $t < t_{g\max}/2$ given as

$$T_a(t) = \frac{1}{2}\left(1 + 2t / t_{g\max}\right) T_{a\max} \text{ at } t < t_{g\max}/2 \text{ and } T_a(t) = T_{a\max} \text{ at } t \geq t_{g\max}/2 \quad (49)$$

Below the given maximal temperature of the anode $T_{a\max}$ is assumed to be equal to the melting temperature of Pd: $T_{a\max} = 1900$ K.

The distribution of the neutral gas is described by the Boltzmann equation as

$$\frac{\partial f_g}{\partial t} + \upsilon \frac{\partial f_g}{\partial x} = -s_i + \mathrm{St}\left(f_g, f_i\right) \quad (50)$$

with f_g the distribution function of the gas and s_i the ionization loss term. The 'Stoβ-term' describes the charge-exchange collisions with ions. Other kinds of collisions between the atoms or ions as well as elastic collisions of atoms with ions and scattering by electrons are not accounted for. The Boltzmann equation for the ion distribution function f_i takes into account the acceleration by the electric field:

$$\frac{\partial f_i}{\partial t} + \upsilon \frac{\partial f_i}{\partial x} + \frac{e}{m_p} E \frac{\partial f_i}{\partial \upsilon} = s_i + \mathrm{St}\left(f_i, f_g\right) \tag{51}$$

If the s_i- and St-terms are known, the problem for Eq. (50) and Eq. (51) is mathematically defined after establishing boundary conditions for f_g and f_i at $x = 0$ and $x = L$. In case of a monotonic electric potential the distribution functions may be defined only for $\upsilon > 0$, but the structure of the developed code is suitable also for calculations with non-monotonic potential in which negative velocities are also possible. For $\upsilon > 0$ the boundary conditions are given at $x = 0$ as $f_i(0, \upsilon) = 0$ for ions and by Eq. (48) for neutrals. For $\upsilon \le 0$ the boundary conditions are established at $x = L$ as $f_g(L, \upsilon) = f_i(L, \upsilon) = 0$.

Density and averaged velocity of ions or atoms are obtained by the integration of their distribution functions as:

$$n_g = \int f_g d\upsilon, \quad n_i = \int f_i d\upsilon, \quad V_g = \int \upsilon f_g d\upsilon, \quad V_i = \int \upsilon f_i d\upsilon \tag{52}$$

Electrons are described, like in the previous modeling, by the hydrodynamics continuity equation in which their averaged velocity is determined by the local electric field taking into account collisions with the neutral atoms occupying the ground state. The continuity equation for electrons is given as

$$\frac{\partial n_e}{\partial t} + \frac{\partial}{\partial x}\left(V_e n_e\right) = S_i \tag{53}$$

The dependencies of the velocity V_e and the ionization source S_i on E/B and on the gas density n_g are discussed in chapter 6. Hence the approach for electrons is valid as long as the plasma, including the quasineutral layer, is weakly ionized: n_i, $n_e << n_g$. In case of monotonic potential electrons always diffuse to the anode, thus $V_e < 0$ and the boundary condition has to be defined only at the cathode. In any case due to the anode sheath at the anode always is valid $E > 0$, i.e. the anode absorbs electrons but doesn't emit them. Thus a boundary condition for electrons at the anode is not necessary.

In solving Eq. (53) it is formally chosen $n_e(L) = 0$ neglecting by this way the density of electrons coming from the cathode. But in the other equations the cathode electrons are accounted for. For the sake of physical clarity the electrons from the cathode and electrons produced by ionization between the anode and the cathode form two different populations. In the thin quasineutral plasma layer of thickness l the density n_{ec} of the cathode electrons becomes much smaller than the density n_e of electrons produced by ionization but in the main volume of the gap the cathode electrons dominate: $n_{ec} >> n_e$ at $l << x < L$. In the modeling it is assumed that due to the development of turbulence in the region of rare plasma outside the quasineutral layer the cathode electrons propagate rather freely through the gap. The dynamics of

electrons in the layer is described by Eq. (53), but the density of the cathode electrons is independent from x due to enhanced turbulent diffusion in the main volume: $n_{ec} = n_{ec}(t)$. The equation for n_{ec} follows from the boundary condition $E(L) = 0$ and is given below.

The expression for s_i is obtained assuming that the ionization rate of atoms doesn't depend on their velocity, thus $s_i \propto f_g$. From this follows:

$$s_i = S_i f_g / n_g \tag{54}$$

The charge-exchange term of Eq. (50) and Eq. (51) is given as

$$\mathrm{St}\left(f_g, f_i\right) = -\mathrm{St}\left(f_i, f_g\right) = \int_0^\infty \sigma_{ce} |\upsilon - \upsilon'| \left(f_i(\upsilon) f_g(\upsilon') - f_g(\upsilon) f_i(\upsilon')\right) d\upsilon' \tag{55}$$

The charge-exchange cross-section σ_{ce} is assumed to not depend on the velocities of the participating particles and is given as $\sigma_{ce} = 5 \cdot 10^{-15}$ cm^2.

The electric field is described by the Poisson equation as:

$$\frac{\partial^2 \varphi}{\partial x^2} = 4\pi e\left(n_e + n_{ec} - n_i\right), \quad \varphi(0) = \varphi_a(t), \quad \varphi(L) = 0, \quad E(L) = -\partial\varphi/\partial x(L) = 0 \tag{56}$$

In the carried out calculations the anode potential $\varphi_a(t)$ of Eq. (56) is given as

$$\varphi_a(t) = \begin{bmatrix} 0 & \text{at } t < t_0 \\ 0.5\left[1 - \cos\left(\pi (t - t_0)/(t_{\max} - t_0)\right)\right]\varphi_{a\max} & \text{at } t_0 < t < t_{\max} \\ \varphi_{a\max} & \text{at } t > t_{\max} \end{bmatrix} \tag{57}$$

Typically the delay time t_0 and the time of reaching the maximal voltage $t_{\max}$ was chosen as $t_0 = 14$ ns and $t_{\max} = t_0 + 50$ ns $= 64$ ns.

The boundary conditions of Eq. (56) over-determine the mathematical problem for the Poisson equation. This allows to find both the electric potential $\varphi(t,x)$ and the density $n_{ec}(t)$. If knowing the functions $n_e(x)$ and $n_i(x)$ as results of solving Eq. (51) and Eq. (53) with the calculation of n_i according to Eq. (52), the Poisson equation is solved integrating Eq. (56) two times over x. After first integration the electric field strength $E = -\partial\varphi/\partial x$ is obtained as:

$$E = E_a + 4\pi e\left(q(x) - n_{ec} x\right), \qquad q(x) = \int_0^x \left(n_i(x') - n_e(x')\right) dx' \tag{58}$$

$E_a \equiv E(0)$. After second integration the potential is obtained as:

$$\varphi(x) = \varphi_a - E_a x + 4\pi e\left(n_{ec} \frac{x^2}{2} - Q(x)\right), \qquad Q(x) = \int_0^x q(x') dx' \tag{59}$$

Considering then Eq. (58) and Eq. (59) at $x = L$ and using the boundary conditions of Eq. (56), a system of two equations for the two unknown variables E_a and n_{ec} is obtained as:

$$E_a = 4\pi e\left(n_{ec}L - q(L)\right), \qquad -\varphi_a + E_a L = 4\pi e\left(n_{ec}\frac{L^2}{2} - Q(L)\right) \tag{60}$$

The solution of Eq. (60) is obtained as

$$E_a = 4\pi e q(L) + \frac{2}{L}\left(\varphi_a - 4\pi e Q(L)\right), \quad n_{ec} = \frac{2}{L}\left(q(L) - \frac{Q(L)}{L} + \frac{\varphi_a}{4\pi e L}\right) \tag{61}$$

9.2. DESCRIPTION OF THE CODE

In order to simplify the algorithm, the self-consistent problem of Eqs. (50), (51), (53) and (59) is solved numerically using the splitting method. During each time step τ the following sub-cycles are completed:

1. Calculation of n_i, V_i, n_g and V_g using f_i and f_g of the previous cycle
2. Calculation of the electric field and the cathode electron density using Eqs. (59) and (61)
3. Ionization sub-step of Eq. (50), Eq. (51) and Eq. (53)
4. Electron convection hydrodynamics sub-step of Eq. (53)
5. Gas convection kinetic sub-step of Eq. (50)
6. Ion convection and ion acceleration joined kinetic sub-step of Eq. (51)
7. Charge-exchange sub-step
8. Correction of spatial meshes

For numerical treatment the coordinates x and υ are simulated with monotonic successions of their values x_k and υ_j at the boundaries of the meshes ($k = 0, 1, .. k_{\max}$; $j = 0, 1, .. j_{\max}$; $0 = x_0 < x_1 < .. < x_K = L$; $\upsilon_{i\min} = \upsilon_0 < \upsilon_1 < .. < \upsilon_{Ji} = \upsilon_{i\max}$). The structure of the numerical grid is shown at Fig. 21. In Fig. 21 the kinetic energy $E_{\text{kin}} = m_p\upsilon^2/2$ is used as axis instead of the velocity υ. In the calculations the maximal spatial mesh index used was $k_{\max} = 100$, the maximal energy mesh index $j_{\max} = 50$, the minimal velocity was $\upsilon_{i\min} = 0$, the maximal velocity $\upsilon_{i\max} \approx 4.5\cdot10^9$ cm/s, corresponding to $E_{\text{kin}} = 10$ MeV. For neutral atoms the same set of spatial meshes and a sub-set of the ion velocity mesh is used: $0 = \upsilon_0 < \upsilon_1 < .. < \upsilon_{Jg} = \upsilon_{g\max}$. The velocities change over rather wide range because for adequate simulation of the distribution function of the entering gas it is necessary to have a relatively small velocity mesh size at small velocities. It was chosen $\upsilon_1 \approx 2.5\cdot10^5$ cm/s, which corresponds to $E_{\text{kin}} \approx 0.037$ eV ≈ 400 K. For this reason a geometric progression of the mesh sizes $\Delta\upsilon_j = \upsilon_j - \upsilon_{j-1}$ is used: $\Delta\upsilon_j = \upsilon_1 q^{j-1}$ with increment factor $q \approx 1.15$. Such a value of q seems quite appropriate to be sure that neighbor meshes have like sizes. The maximal gas velocity mesh index used was $j_{g\max} = 20$ corresponding to the maximal kinetic energy of atoms of 360 eV. This is sufficient for an adequate representation of the distribution function of the atoms.

For the size of the spatial meshes a mesh correction procedure is used being described below in detail. Change of the mesh sizes in the course of the calculation is necessary because of the existence of a rather thin electrostatic sheath at the cathode

edge of the quasineutral layer. The ions are extracted from this edge and accelerated through the gap by the electric field. In the course of the diode operation cycle the cathode edge gradually moves along the x-axis, thus the region of denser meshes should follow the edge. For the sheath located near the anode there is no mesh size problem if using the geometric progression for the sizes $\Delta x_k = x_k - x_{k\text{-}1}$ of initial spatial mesh as $\Delta x_k = x_1 p^{i-1}$ with $x_1 = 10^{-4}$ cm and the increment factor $p \approx 1.07$. Hence in order to make the meshes denser the region including the cathode edge is slightly corrected after each time step. But far enough from the edge during the run the geometric progression sizes are kept.

9.2.1. CALCULATION OF HYDRODYNAMICS MOMENTS

The moments are given as:

$$n_{\alpha k} = \sum_{j=1}^{j_{\alpha\max}} f_{\alpha kj} \Delta \upsilon_j , \qquad V_{\alpha k} = \sum_{j=1}^{j_{\alpha\max}} \upsilon_{mj} f_{\alpha kj} \Delta \upsilon_j \tag{62}$$

with the substance index $\alpha = i$ or g , $n_{\alpha k} = n_\alpha(x_{mk})$ the substance density in the center of the k-th spatial mesh, $V_{\alpha k} = V_\alpha(x_{mk})$ substance velocity at the center, $f_{\alpha kj} = f_\alpha(x_{mk}, \upsilon_{mj})$ the substance distribution function at the center. The center coordinate $x_{mk} = (x_{k-1}+x_k)/2$, the velocity in center of j-th velocity mesh $\upsilon_{mj} = (\upsilon_{j-1}+\upsilon_j)/2$. It is valid $j_{\max} \equiv j_{i\max}$. The moments and the distribution functions are calculated from the previous time step.

9.2.2. ELECTRIC FIELD CALCULATION

Because the Poisson equation is already solved, Eq. (59) is rewritten as an expression for the electric potential $\varphi_k = \varphi(x_k)$ in terms of the numerically calculated integrals for $q_k = q(x_k)$ and $Q_k = Q(x_k)$ at the boundaries of the meshes as:

$$\varphi_k = \varphi_a - E_a x_k + 4\pi e\left(n_{ec}\, x_k^2/2 - Q_k\right) \tag{63}$$

The anode electric field E_a and the cathode electron density and n_{ck} are given by Eq. (61) at $Q(L) = Q_K$, $q(L) = q_K$. It is valid $K \equiv k_{\max}$, $Q_0 = 0$, $q_0 = 0$. The numerical integrals are given as

$$Q_k = \sum_{m=1}^{k} \frac{q_{m-1} + q_m}{2} \Delta x_m , \qquad q_k = \sum_{m=1}^{k} \left(n_{im} - n_{em}\right) \Delta x_m , \quad k = 1, 2, .. k_{\max}, \tag{64}$$

The electric field strength at the mesh centers is calculated as $E_k = (\varphi_{k-1} - \varphi_k)/\Delta x_k$. In the calculation of q_k the densities n_i and n_e from the previous time step are used.

9.2.3. IONIZATION SUB-STEP

The change of the electron density and the distribution functions of ions and neutral atoms caused by ionization is calculated using the explicit scheme as:

$$\frac{n_{ek1}-n_{ek}}{\tau}=w_k, \qquad \frac{f_{gkj1}-f_{gkj}}{\tau}=-\frac{w_k}{n_{gk}}f_{gkj}, \qquad \frac{f_{ikj1}-f_{ikj}}{\tau}=\frac{w_k}{n_{gk}}f_{gkj} \tag{65}$$

Here the index 1 denotes the results of the ionization sub-step obtained after calculation for Eq. (65), $w_k=(n_{ek}+n_{ec})\nu_i(E_k,n_{gk})$. The ionization frequency ν_i is obtained from a table of the ionization frequencies. This table is calculated as described in chapter 6.

9.2.4. SUB-STEP FOR ELECTRON CONVECTION

At this sub-step the electron density gets an additional change in accordance with the contribution of the convective term of Eq. (53). The density change is calculated using the implicit scheme as:

$$\frac{n_{ek2}-n_{ek1}}{\tau}+\frac{n_{e(k+1)2}V_{e(k+1)}-n_{ek2}V_{ek}}{\Delta x_k}=0 \tag{66}$$

The index 2 denotes the results of this sub-step, the hydrodynamics electron velocity $V_{ek}=V_e(E_k,n_{gk})$ is obtained from the table obtained in chapter 6 together with the ionization frequency. The 'shifted to the right' numerical scheme is applied according to the motion of electrons to the left. Namely such scheme is necessary from physical point of view because the electrons come through the right boundary x_k of k-th cell thus bringing the information about (k+1)-th cell by the values $n_{e(k+1)}$ and $V_{e(k+1)}$. The scheme of Eq. (66) is conservative. This means that the whole number of electrons in the gap changes only due to the fluxes of electrons through the anode or due to the cathode electrons. The hyperbolic scheme of Eq. (66) needs only a boundary condition at $k=K$. This condition is given as $n_{eK2}=0$. The values of the density are obtained from Eq. (66) completing the recurrence cycle for $k=1, 2, .. K$-1 as:

$$n_{ek2}=\frac{n_{ek1}-(\tau/\Delta x_k)n_{e(k+1)2}V_{e(k+1)}}{1-(\tau/\Delta x_k)V_{ek}}, \qquad n_{eK2}=0 \tag{67}$$

It should be noted that an additional investigation of the transition region with sharp gradients at the cathode edge of the quasineutral layer is desirable aiming in elimination of numerical oscillations there, which are obtained in the calculations. However those oscillations cannot make the conservative solution wrong, therefore their elimination is not urgent. Further discussion on how separate the regions of the anode plasma and the cathode sheath in numerical calculations is given in chapter 12.

9.2.5. GAS CONVECTION SUB-STEP

The density of the neutral gas changes at this sub-step according to the convective term of Eq. (50):

$$\frac{f_{gkj2}-f_{gkj1}}{\tau}+\upsilon_j\frac{f_{gkj2}-f_{g(k-1)j2}}{\Delta x_k}=0 \tag{68}$$

The index 2 denotes the results of this sub-step. Eq. (68) describes the implicit scheme equation solved recurrently as

$$f_{gkj2} = \frac{f_{gkj1} + \left(\tau v_j / \Delta x_k\right) f_{g(k-1)j2}}{1 + \tau v_j / \Delta x_k} \tag{69}$$

The boundary condition for Eq. (69) is given at $k = 0$ using the Maxwellian function of Eq. (48) with the anode temperature and the anode gas flux given at this sub-step.

9.2.6. ION CONVECTION SUB-STEP

The convective dynamics of ions and their acceleration by the electric field is described simultaneously by the following implicit scheme:

$$\frac{f_{ikj2} - f_{ikj1}}{\tau} + v_j \frac{f_{ikj2} - f_{i(k-1)j2}}{\Delta x_k} + \frac{e}{m_p} E_k \frac{f_{ikj2} - f_{ik(j-1)2}}{\Delta v_j} = 0 \tag{70}$$

The index 2 denotes the results of this sub-step. The recurrent solution of Eq. (70) is obtained as

$$f_{ikj2} = \frac{f_{ikj1} + \left(\tau v_j / \Delta x_k\right) f_{i(k-1)j2} + \left(\tau e E_k / m_p \Delta v_j\right) f_{ik(j-1)2}}{1 + \tau v_j / \Delta x_k + \tau e E_k / m_p \Delta v_j} \tag{71}$$

Boundary condition for Eq. (71) are given at $j = 0$ as $f_{ik0} = 0$ and at $k = 0$ as $f_{i0j} = 0$.

9.2.7. CHARGE-EXCHANGE SUB-STEP

At this sub-step the contribution of the St-term to Eqs. (50) and (51) is calculated using the following implicit scheme:

$$\frac{f_{gkj3} - f_{gkj2}}{\tau} = f_{ikj3} \nu_{gkj} - f_{gkj3} \nu_{ikj}, \qquad \frac{f_{ikj3} - f_{ikj2}}{\tau} = f_{gkj3} \nu_{ikj} - f_{ikj3} \nu_{gkj} \tag{72}$$

The index 3 denotes the results of this sub-step. Collision frequencies are given as

$$\nu_{\alpha kj} = \sigma_{ce} \sum_{m=1}^{J_g} \left| v_j - v_m \right| f_{\alpha km2} \Delta v_m \ (\alpha = i \text{ or } g) \tag{73}$$

The linear system of Eq. (72) for f_{gkj3} and f_{ikj3} is solved resulting in

$$f_{ikj3} = d^{-1}\left(f_{ikj2} + \nu_{ikj}\tau\left(f_{ikj2} + f_{gkj2}\right)\right), \quad f_{gkj3} = d^{-1}\left(f_{gkj2} + \tau\nu_{gkj}\left(f_{ikj2} + f_{gkj2}\right)\right) \tag{74}$$

The factor d is given as $d = 1 + (\nu_{ikj} + \nu_{gkj})\tau$.

9.2.8. CORRECTION OF SPATIAL MESHES

This sub-step is activated after formation of a rather narrow layer of quasineutral plasma. This happens at $\varphi_a \approx 10^2$ kV. The edge position of the layer from the cathode side is defined as the center of a mesh in which the electric field strength changes most significantly. The criterion for the edge position is defined via the maximum of the special function $\chi(x)$ given in the mesh centers as

$$\chi_k = \left| \frac{E_{k+1} - 2E_k + E_{k-1}}{E_{k+1} + 2E_k + E_{k-1}} \right| \qquad (k = 1, 2, .. 3K/4) \tag{75}$$

The index of the mesh of the edge position is designated as k_c. At $k = k_c$ the meshes are most dense as it is shown in the central part of the Fig. 21.

The sizes of the meshes surrounding the edge position are decreased at each time step according to

$$\left(1 - 0.3\frac{\tau}{0.05\,\text{ns}}\exp\left(-\frac{|k - k_c|}{10}\right)\right)\Delta x_k \to \Delta x_k \tag{76}$$

Thus the size decrease is more significant for mesh indexes k being near k_c.

For keeping the sizes of the more distant meshes the following transformation is used:

$$\Delta x_k + \varsigma\left(\Delta x_{k0} - \Delta x_k\right) \to \Delta x_k \tag{77}$$

with Δx_{0k} the initial (corresponding to the start of calculation) geometric progression succession. The factor ς is obtained from the requirement of keeping the gap size as:

$$\sum_{k=1}^{K} \Delta x_k = L \tag{78}$$

By this way new mesh boundary coordinates x_{nk} are obtained for the next time step. Redistribution of $n_e(x)$ and $f_\alpha(x,v)$ to the new meshes is provided keeping the conservation of particles by introducing the particle number functions as:

$$N_e\left(x_{ok}\right) = \sum_{m=1}^{k} n_{eom}\Delta x_{om}\,, \qquad F_{\alpha j}\left(x_{ok}\right) = \sum_{m=1}^{k} f_{\alpha omj}\Delta x_{om} \tag{79}$$

The index o denotes the old values obtained after the previous sub-steps. The particle number functions are linearly approximated at the new mesh boundaries, e.g. as:

$$N_e\left(x_{nk}\right) = N_e\left(x_{o(m-1)}\right) + \left(N_e\left(x_{om}\right) - N_e\left(x_{o(m-1)}\right)\right)\frac{x_{nk} - x_{om}}{\Delta x_{om}} \tag{80}$$

It is valid $x_{o(m-1)} \le x_{nk} < x_{om}$. Finally the new densities and the distribution functions are obtained as

$$n_{ek} = \frac{N_e\left(x_{nk}\right) - N_e\left(x_{n(k-1)}\right)}{\Delta x_{nk}}, \quad f_{\alpha kj} = \frac{F_{\alpha j}\left(x_{nk}\right) - F_{\alpha j}\left(x_{n(k-1)}\right)}{\Delta x_{nk}} \tag{81}$$

The schemes used in the calculation are stable as long as the time increment τ is small enough. The calculations have been carried out with time step of value $\tau \geq 10^{-3}$ ns.

10. RESULTS OF NUMERICAL CALCULATIONS

Initially (at time $t = 0$) the diode gap is empty. There is no voltage applied between the electrodes. At $t > 0$ the voltage is still zero but the anode plate is becoming gradually heated resulting in the appearance of vaporized neutral hydrogen atoms in the gap. After some time delay t_0 the voltage starts to increase, thus an electric field appears between the electrodes. In the course of the increase of the electric field strength E the electrons coming from the cathode are occupying uniformly the whole gap and providing the necessary boundary condition at the virtual cathode $E(L) = 0$. The cathode is assumed to be motionless in the considered scenario because for taking into account its motion the spatial variation of B has to be calculated[13]. Electrons coming from the cathode produce impact ionization of the vaporized gas. Afterwards the secondary electrons also participate in the ionization. As a result a dense quasineutral plasma layer develops near the anode. The self-consistent electric field E decreases in the quasineutral layer drastically. The electrons diffuse slowly through the layer and across the lines of the applied magnetic field to the anode. The ions are flowing through the layer in the reverse direction being slowed down by the charge-exchange collisions. The ions arriving at the cathode edge of the quasineutral layer are extracted by a strong edge electric field and are accelerated across the gap to the cathode. The increase of the electric field strength at the cathode edge due to the increase of the voltage causes the increase of ion extraction from the anode plasma. This results in a regime where the self-consistent electric field strength becomes too small for compensation of the ion extraction by ionization in the anode sheath and in the quasineutral layer. Thus starts an operational phase in which the layer provides the necessary Child-Langmuir ion flux mainly due to its erosion. Due to that in the course of the voltage increase the layer becomes thinner and finally disappears. After this the electric current through the diode decreases by orders of value because of rather weak ionization in strong electric field at $E >> 10^5$ V/cm according to the analysis of chapter 6.

Acceptable regimes of diode operation correspond to the disappearance of the anode plasma after the moment of reaching the maximal voltage. Calculating with different delay times t_0 it was discovered that the longer t_0 the later the anode plasma exhaustion. Thus the regimes with the exhaustion of the anode plasma at the moment of reaching the maximal voltage establish the minimal delay times.

Such a scenario with the minimal t_0 is demonstrated in Figs. 22 – Fig. 29 for a gap width of $L = 1$ cm. The anode voltage φ_a starts with t_0 of 50 ns and then rises during 50 ns up to $\varphi_{max} = 5$ MV (in the figures φ_{max} is designated as U_{max}). Similar scenarios for other maximal voltages have been calculated as well. As examples, Figs. 30 – 33 show the evolution of the ion density and of the electric fields for $\varphi_{max} = 1$ and 2 MV, and Figs. 34 and 35 show the distribution functions of ions and

neutral atoms for φ_{max} = 1 MV. In Table 2 the dependence of the minimal delay time t_0, the maximal ion density in the quasineutral layer and the maximal electron density in the gap on φ_{max} are presented.

Independently from φ_{max} the gas vaporization flux from the anode reaches its maximum after t = 20 ns after starting the heating of the Ti–Pd film and then remains constant. The voltage applied across the gap starts after $t = t_0$ and reaches $\varphi_a = \varphi_{max}$ at $t = t_{max} = t_0 + 50$ ns (see Fig. 22). During most time within the time interval (t_0, t_{max}) the fluxes of ions and electrons through the diode rise up according to the Child-Langmuir law of Eq. (11). The quasineutral layer exists during the current increase and thus provides the boundary condition with a small electric field at the anode plasma edge. The electron flux only weakly exceeds the ion flux due to the contribution of electrons from the cathode (Fig. 23).

The formation of the self-consistent electric field in the anode plasma is shown in Fig. 24. Initially (at $t \le 52$ ns) only the electrons coming from the cathode determine the behavior of the electric field. They homogeneously occupy the main volume of the gap (see Fig. 25) and thus provide the boundary condition $E = 0$ at the virtual cathode. At later times due to ionization in the vaporized gas the anode plasma appears. The applied electric field causes charge separation in the plasma and thus the development of the reversed induced electric field. The composition of the applied and the induced electric fields constitutes the self-consistent electric field. Because of rather small values of the self-consistent electric field, charge separation in the anode plasma results in a practically complete compensation of the applied field by the induced field in the region of the anode plasma as is clearly seen from Fig. 24. As shown in Fig. 25, during the anode plasma formation phase (at $50 < t < 60$ ns) a quasineutral layer of thickness of about 0.5 mm forms. It is enveloped from both sides by the anode sheath and by the ion accelerating cathode sheath. In the sheaths the quasineutrality fails. Charge separation is seen as an accumulation of negative charge in the anode sheath (because there is valid $n_e > n_i$) and of positive charge at the opposite side of the quasineutral layer (because there is valid $n_e < n_i$). Due to the small magnitude of the electric field at the cathode edge of the anode plasma and at the cathode the whole electric charge of the main volume of the gap is negligibly small. Thus averaged ion density there is equal to the density n_{ec} of electrons coming from the virtual cathode.

Figs. 26 and 27 show the exhaustion phase. In the quasineutral layer the self-consistent electric field changes reversely to the drastic rise of the gap voltage. Without the preliminary qualitative analysis would be impossible to explain such behavior. This occurs due to the non-exponential increase of the anode plasma density in the course of ionization in the self-consistent electric field. If the electric field in the layer would be constant the ionization would result in an exponentially fast rising anode plasma density, which could be possible only at exponentially rising voltage as was analyzed in the first part of this work. But in the numerical calculation the voltage increase remains below an exponential increase. Thus the ionization increase also remains below an exponentially rising function. To provide such a behavior the self-consistent field automatically decreases in the course of the diode operation. Characteristic values of the self-consistent electric field are of the order of 3 – 7 kV/cm (see Fig. 26). According to Fig. 9 this corresponds to the mean kinetic energy of electrons in the anode plasma of 7 – 10 eV.

The maximal density of the anode plasma is of $7 \cdot 10^{15}$ cm^{-3}. According to Fig. 28 the density of the neutral hydrogen is by a factor of 50 larger than the plasma

density. Thus the anode plasma is weakly ionized. The thickness of the layer of the vaporized gas is much larger than the thickness of the anode plasma. However the thickness ratio depends on the regime of the voltage increase. As was shown analytically in the first part the thickness ratio is of 1 for the regime with the exponential increase of the voltage at least for an initial stage without sufficient erosion at the cathode edge.

Mean velocities of ions and of neutral atoms are shown in Fig. 29. The ions produced by ionization in the anode sheath move rather evenly and slowly through the quasineutral layer with the velocity of 1÷2 cm/μs. Finally they cross the edge of the anode plasma and accelerate in the gap. The neutral atoms increase their velocity due to charge exchange process schematically shown in Fig. 16. The velocities of the neutrals in the gap are of 10^7 cm/s thus corresponding to the neutral kinetic energies of 10^2 eV. According to Fig. 28 the neutral density in the gap is of the order of 10^{15} cm^{-3} thus being several orders of magnitude smaller than in the layer of the vaporized gas near the anode but significantly larger than the averaged densities of ions and the cathode electrons.

The calculations with lower maximal voltages (1 and 2 MV) showed a rather similar behavior of the anode plasma. As it follows from the values of the ion density shown in Figs. 30 and 32 the anode plasma is always weakly ionized. The self-consistent electric field shown in Figs. 31 and 33 also decreases down to 7 and finally to 3 kV/cm thus resulting in an effective electron temperature in the quasineutral layer of around 7 – 10 eV.

Examples of 2 dim ion and neutral distributions in the gap are given in Figs. 34 and 35 for φ_{max} = 1 MV. They are rather similar for 2 and 5 MV. In Fig. 34 there are seen two regions in the ion distribution. At low velocities ions mainly are located in the thin quasineutral layer. Here maximal values are reached. In the main volume of the gap the accelerated ions as seen in Fig. 34 are forming a beam. In reality the width of the accelerated ion beam at the velocity axis should be narrower as shown in Fig. 34 where numerical diffusion slightly broadens the ion distribution. The position of the anode plasma edge is the starting position of the accelerated ions. This is seen in Fig. 34 as the edge of the ion distribution at small velocities. In Fig. 35 the influence of charge exchange processes on the distribution of neutrals is seen as a widening of the distribution function at enlarged velocities. The energetic tail of the distribution function shows similarities to the ion distribution shown in the previous picture. Thus charge exchange contributes also in the cathode sheath near the anode plasma region. By comparing Figs. 34 and 35, it is seen that the position of the edge of the neutral distribution is located deeper in the gap as that of the ion distribution.

Concerning the position of the edge of the neutral distribution, three mechanisms principally are influencing the numerical results. These are the penetration of the neutrals acquiring sufficient velocity in the quasineutral layer into the gap, the free expansion of the neutrals vaporized from the anode at $t << t_0$ across the gap and numerical diffusion. Presently a clear discrimination between the different contributions of these mechanisms is not possible.

11. COMPARISON WITH EXPERIMENTS

The main objective of this work is to demonstrate a consistent but preliminary modeling for applied–B ion diodes. At the level achieved up to now it would be too

ambitious to simulate existing installations. Therefore only some first remarks concerning the relation of the obtained numerical results to available measurements on the anode plasma in applied–B ion diodes are given. As source of experimental information Refs. 2–5 are analyzed with respect to electron and hydrogen components in the discharges. Results related to discharge impurities are not commented here.

In Ref. 2 spectroscopic measurements were carried out. On the base of the Seeman splitting of atomic energy levels the electron density and the electron temperature in the anode plasma were estimated. For this reason the applied magnetic field B in the gap was measured. During the pulsed gap voltage of $\varphi_{max} \approx 1.7$ MV with pulse front time of 30 ns the magnitude of B was changing from 3 T up to 5 T. The anode plasma is created after application of a preliminary electric pulse to the ends of the anode plate in order to breakdown hydrogen released after heating of the Ti-Pd film as is described in chapter 2. Both heating and breakdown voltages are applied parallel to the anode plate and are independent on the gap voltage. From the measurements it was concluded that the electron temperature in the discharge rises fast up to 7 eV and then keeps rather constant. During the operation the hydrogen atomic density continuously increased and the averaged electron density of the anode plasma was risen from 10^{16} up to $5 \cdot 10^{17}$ cm^{-3}. The divergence of the ion beam in the gap was determined from the Doppler frequency shift of the line radiation. It was concluded that a considerable part of the divergence is already created at the anode plasma edge thus indicating a rather inhomogeneous edge surface.

In Ref. 3 details on evolution of B and of electron density are discussed. Initially the magnitude of B increases from 1.9 T at the cathode up to 3.3 T at the anode over the gap of width of 8.5 mm. Thus at the beginning of the pulse the field B is not uniform in the gap. The anode plate width is given as 2.7 cm and the anode emission area as 123 cm^2. The gap voltage rises from zero up to 2 MV during the first 40 ns and then decreases again to zero during the next 60 ns. During the whole 100 ns the ion beam current rises up to 0.5 MA. This information is useful in future adjustments of the calculations to the experimental conditions. The electron density in the gap was measured by interferometer. Farther than 3 mm from the anode it is homogeneous and rises up to $2 \cdot 10^{13}$ cm^{-3} during first 30 ns and then keeps constant for about 20 ns. At the following decrease of the voltage the density at the center of the gap continues to increase reaching finally the magnitude of $7 \cdot 10^{13}$ cm^{-3}. At the stage of the voltage decrease the density is inhomogeneous. It gets minimal at the gap center and larger of a factor of 3÷5 near the electrodes. At a distance to the anode less than 0.7 mm the density drastically rises up reaching the upper measurement limit of $2 \cdot 10^{14}$ cm^{-3} during first 15 ns and then always remains larger. At the distance of 1 mm the density rises up during the first 10 ns, then reaches a maximum of $7 \cdot 10^{13}$ cm^{-3} and then decreases down to $(1 \div 2) \cdot 10^{13}$ cm^{-3} after the next 20 ns. The density behavior during the stage of the voltage decrease is not presented. At the distance of 2 mm the behavior of the density is rather similar to that for 1 mm but the maximum is lower ($3 \cdot 10^{13}$ cm^{-3}) and, after the density decreased, it starts to increase again up to values larger than 10^{14} cm^{-3}. Thus the behavior gets more similar to those in the gap. The density behavior near the anode (up to 1 mm) is explained for the stage of the voltage increase in terms of the moving edge due to the anode plasma expansion and erosion. From the measurements of the dispersion coefficient it was concluded that the plasma in the gap is ‘rather cold’.

In Refs. 4 and 5 the anode plasma is formed over a dielectric surface. The maximal voltage φ_{max} was 0.27 MV, the applied magnetic field 0.5 - 1 T and the gap width 8 mm. At 30 ns the plasma occupies a pre-anode region of 1.5 mm width. The kinetic energies of protons and electrons were found to be of 5 – 8 eV. The ions acquire their energy within 10^{-2} cm from the anode. The expansion velocity of the anode plasma V_{exp} was 3 cm/μs and the plasma density $3 \cdot 10^{15}$ cm^{-3}. A reference to another work[24] was done where for φ_{max} with 0.7 MV the density was measured to be $4 \cdot 10^{16}$ cm^{-3} and V_{exp} 2 cm/μs. It was concluded that classical diffusion doesn't explain such expansion velocities. They were attributed to anomalous diffusion caused by the lower hybrid drift instability.

A comparison of available experimental plasma parameters with those obtained in this work is presented in Table 3. The 'effective electron temperature' T_e is in good agreement with all mentioned experiments on the applied–B ion diodes both for the pre-anode discharge and for the flashover anode plasma. This indicates that the model of electron motion in crossed electric and magnetic fields, presented in chapter 6, is rather adequate for the problem under investigation. The difference of a factor 4 in the electron densities in the gap n_{egap} can be easily explained by different gap sizes, which would increase the calculated density by a factor $(1/0.85)^2 \approx 1.4$, and by approaching of the virtual cathode to the anode due to diamagnetic effects in the experiment, which was not taken into account in the calculations.

The calculated electron density of the anode plasma differs drastically from the experiments. The maximal numerical magnitude of n_e in Table 2 corresponds to φ_{max} of 5 MV being of the order of experimental results as measured for φ_{max} with 0.27 MV. The difference at comparable values of φ_{max} is more than one order of magnitude. The explanation of the difference now may be only speculative. Perhaps the reason is ignoring in modeling the impurities, which are ionized much easier than atomic hydrogen thus providing faster ionization during the pulse time of several tenths of nanoseconds. Another reason is that much larger amount of anode plasma can be created before application of the gap voltage because of preliminary ionization in the parallel electric field, which is not implemented in modeling. The difference of factor 3 - 5 in the thickness of the anode plasma can also be caused by the absence of mentioned ionization mechanisms in the modeling. Perhaps the rise up behavior of the gap voltage also influences significantly the thickness. Because the difference in the anode plasma thickness for the cases of exponential and sinusoidal voltage rise up obtained in calculations indicates important role of the voltage drive for the plasma thickness.

The plasma expansion velocity often is interpreted in terms of fluid models as the velocity V_i of ions coming off the anode. With such an interpretation the plasma expansion across the magnetic field lines should be attributed to anomalous diffusion because with classical diffusion V_{exp} would be smaller than in experiments by an order of magnitude. In the modeling presented no anomalous diffusion was implemented but ions were calculated in a rather general way by solving the kinetic equation with charge exchange St-term as discussed in chapter 9. According to the numerical results, the plasma expansion arises due to formation of a plasma layer with increasing thickness in external electric field applied to the previously expanded gas layer of neutrals. Thus the plasma front expansion doesn't concern motion of plasma particles. As it is clearly seen from Table 2, the magnitude of V_{exp} in the presented modeling is obtained to be of the experimental one. This indicates that turbulent diffusion of the anode plasma might be absent. The calculated ion velocity V_i, which

is formed in the quasineutral layer by charge-exchange processes, is in rather good agreement with the experimental value.

12. NECESSARY MODEL IMPROVEMENTS

A still more realistic ion diode simulation requires implementation of the following physical processes into the presently existing code:

1. The dynamics of the magnetic field $\mathbf{B}(t,x)$ (diamagnetic effect)
2. The motion of the virtual cathode towards the anode
3. The dynamics of impurities in the anode plasma

More attention has to be paid to the voltage drives in order to understand properly its influence for the expansion velocity of the anode plasma. The calculations have to be carried out with larger delay times thus investigating anode plasmas with larger densities and larger thickness being closer to the presently performed experiments. However it seems that the regimes resulting in the exhaustion of the anode plasma at approaching the maximal voltage may be also interesting for further investigations. After exhaustion the diode current interrupts in a few nanoseconds. If such effect would be discovered experimentally, the finding may be used for amplification of the maximal voltage by means of including an additional conductivity in the diode circuit.

Taking into account impurities will approach the goal of using the code for interpretation of the spectroscopy measurements because radiation spectra of impurities can be calculated. This task will require the self-consistent calculation of the dynamics of the excited levels influenced by collisions and radiation decay. An appropriate solver for such problem is available[25].

Concerning the further development the following should be investigated additionally. The principal similarity of discharges in parallel and perpendicular electric fields mentioned in chapter 2 is substantiated in the following way. At a very early stage the electric field in the gap is an externally applied field, thus its spatial shape is determined by the boundary conditions at the surrounding electrodes. After the development of the quasineutral layer the electric field is becoming a self-consistent field, thus its shape is determined mainly by the quasineutral layer playing the role of an additional 'plasma electrode' in the gap. A qualitative example of the shape of the initial electric field and of the field after the development of the quasineutral layer is shown in Fig. 36 for a case with the auxiliary voltage $\varphi_{\|}$ applied to the ends of the anode plate. By this way an electric field initially parallel to the anode is produced. The quasineutral layer may be modeled as a volumetric electrode having approximately constant electric potential of $\varphi_{\|}/2$ along the field lines of the applied magnetic field **B**. The electric current is going along the anode plate (I_a, as it is shown in Fig. 36) and along the quasineutral layer (I_p). For a developed quasineutral layer of impedance smaller than that of the anode plate it is valid $|I_p| > |I_a|$. The quasineutral layer electrically contacts the ends of the anode plate where the electric field is rather perpendicular to **B**. Hence during the most important stage with applied accelerating voltage φ_a and developed quasineutral layer the processes analyzed in this work should be valid also for the case with an initially parallel electric field. But from the discharge geometry schematically shown in Fig. 36 it is clear that an adequate description of this case is a spatial 2 dim problem having to be also investigated in future.

In order to avoid numerical oscillations at the cathode edge of the anode plasma (see Fig. 26), the meshes for the gap and for the anode plasma should be separated. A possible way how to do this is suggested considering a rather small part of the gap around the edge. The extracted ion flux j_i is assumed to be given by Eq. (11). Physical parameters at the edge position are given below with zero index. The edge electric field E_0 inside of the quasineutral layer causes a flux j_{i0} of ions from the depth of the anode plasma. These ions are produced in the pre-anode electrostatic sheath and in the quasineutral layer. In case without edge erosion it is valid $j_{i0} = j_i$ but generally $j_{i0} < j_i$ because due to the erosion a part of the extracted ions starts from the edge. Thus it is valid

$$j_i = j_{i0} - n_0 V_0 \tag{82}$$

with n_0 the density of the quasineutral plasma at the edge and V_0 the erosion velocity ($V_0 < 0$). The ions of the eroding quasineutral plasma edge after separation from electrons accelerate across the gap but electrons remain at the moving edge thus their hydrodynamics velocity υ_e is equal to V_0.

The density n_0 is determined by the previous ionization in the quasineutral layer described by Eq. (7) thus at the analysis of the edge n_0 is given. The parameters j_{i0} and V_0 with $V_0 = \upsilon_e$ are obtained from the equations of motion Eqs. (9) and (23) at the current edge position. The field E_0 drags the electrons towards the anode thus the velocity V_0 is given as $V_0 = -\mu E_0$ with μ the electron mobility coefficient (see chapter 7) determined by their gyration motion in the applied magnetic field and by their collisions with the neutrals, which are assumed to occupy a rather wide region near the anode. Also E_0 drags the ions in the opposite direction. The ions colliding with neutrals undergo charge exchange. Their flux j_{i0} is given as $j_{i0} = n_0(eE_0\lambda_i/2m_a)^{1/2}$.

Subsituting the given expressions for j_{i0} and V_0 into Eq. (82), the equation for E_0 is obtained as $\mu E_0 + (eE_0\lambda_i/2m_a)^{1/2} - j_i/n_0 = 0$. Its solution is given as

$$E_0 = \left(\left(\frac{e\lambda_i}{8m_a\mu^2} + \frac{j_i}{n_0\mu} \right)^{1/2} - \left(\frac{e\lambda_i}{8m_a\mu^2} \right)^{1/2} \right)^2 \tag{83}$$

Using E_0 of Eq. (83), the erosion velocity of the edge and the ion flux j_{i0} are obtained. By this way the problem for the anode plasma is provided with the necessary boundary conditions at the edge for electric field E as $E|_{\text{edge}} = E_0$ and for the edge velocity as $V|_{\text{edge}} = V_0$ thus separating the numerical problem for the anode plasma from that of the gap with fitting their boundary.

The problem of anode plasma stability is not considered in this work. According to Ref. 2 the plasma edge can become unstable thus this problem is important for focusing of the accelerated ion beam. A first step in this direction would be the analysis of small perturbations starting from solutions provided by the described code. In case of evolving instabilities of the anode plasma a code with 2 spatial dimensions has to be developed. Such a code would allow to investigate non-linear stages of the instabilities. For the development of such a code the discussed above fitting the boundary of the anode plasma and the gap region seems to be necessary.

13. CONCLUSIONS

The mechanisms of ion flux production in the anode plasma are analyzed using an analytical approach for rather moderate values of the diode voltage ($\varphi_{max} \leq 1$ MV) in the first part of the work. In the second part numerically the anode plasma is investigated for values of φ_{max} from 1 MV up to 5 MV. In the first part the modeling with exponentially increasing voltage at the given profile of the neutral density near the anode is carried out and the erosion of the anode plasma is neglected. In this case the thickness of the anode plasma is of the thickness of the given layer of neutrals. In the second part a consistent 2 dim model of the anode plasma is developed. Filling of the pre-anode space with neutrals is implemented using the results of an independent analysis of hydrogen diffusion in the Ti–Pd film structure covering the anode plate. Formation and behavior of the quasineutral anode plasma layer are analyzed in detail calculating both the plasma kinetic dynamics and the self-consistent electric field in the gap and in the anode plasma. The charge exchange dynamics of neutrals in the gap is coupled with the ion dynamics. In contrast to the results of the first part, the thickness of the anode plasma is obtained to be much less than the thickness of the layer of neutrals produced by the accompanying vaporization near the anode. The erosion at the edge of the anode plasma causes this difference. The anode plasma is always weakly ionized. Charge-exchange processes in the quasineutral layer are producing neutral atoms of energies of 10^2 eV. The electrostatic sheaths adjacent to the anode and at the cathode edge of the anode plasma are the main regions of ion flux production. A regime with complete exhaustion of the anode plasma when reaching the maximal voltage is found. Minimum delay times between start of the heating of the hydride film and application of the gradually increasing accelerating voltage are obtained. At smaller delay times a fast interruption of the diode current would occur before reaching the maximal voltage. Finally comparing the numerical results with available experimental data a good agreement with the experiments for the effective electron temperature and the ion velocity in the anode plasma is obtained. The obtained disagreement for the plasma density and the plasma thickness requires further development of the modeling. The next steps for improvement of the anode plasma numerical simulations are discussed.

14. ACKNOWLEDGEMENT

The authors would like to thank H.J. Bluhm from Forschungszentrum Karlsruhe – IHM for stimulating discussions and advice on all aspects of the physics of high power ion diodes.

15. REFERENCES

1. S. Humphries, Jr., 'Intense pulsed ion beams for fusion applications', Review paper, Nucl. Fusion 20, 1549 (1980)
2. Suk-Jae Yoo, 'Spektroskopische Messungen im Anodenplasma einer isolierten Hochleistungs-Ionendiode', FZKA 5976, Forschungszentrum Karlsruhe, 1997
3. V. Licht, 'Messung der Elektronendichte im Beschleunigungsspalt von Hochleistungsionendioden mit Hilfe eines hochempfindlichen Zweiwellenlängen-Dispersions-Interferometers', FZKA 6293, Forschungszentrum Karlsruhe, 1999
4. Y. Maron et al., 'Particle-velocity distribution and expansion of a surface-flashover plasma in the presence of magnetic fields', Phys. Rev. A, 39, 5842 (1989)
5. Y. Maron et al., 'Electron temperature and heating processes in a dynamic plasma of a high power diode', Phys. Rev. A, 40, 3240 (1989)
6. J.E. Maenchen at el. 'Extreme-ultraviolet illumination effects of the PBFA-I magnetically insulated ion diode', J. Appl. Phys. 65, 448 (1989)
7. D.J. Johnson, J.P. Quintenz, and M.A. Sweeney, 'Electron and ion kinetics and anode plasma formation in two applied B_r field ion diodes', J. Appl. Phys. 57, 794 (1985)
8. J.B. Greenly, M. Ueda, G.D. Rondeau, and D.A. Hammer, 'Magnetically insulated ion diode with a gas-breakdown plasma anode', J. Appl. Phys. 63, 1872 (1988)
9. H.J.Bluhm, H.P.Laqua, L.Buch, P.J.W.Hoppė, D.Rusch. 'Formation of a homogeneous hydrogen plasma layer for the production of terawatt ion beams. IEEE transactions on plasma science', 21, 560 (1993)
10. H.P. Laqua, H.J. Bluhm, L. Buch, and P. Hoppė, 'Properties of the non-equilibrium plasma from a pulsed sliding discharge in a hydrogen gas layer desorbed from a metal hydride film', J. Appl. Phys. 77, 5545 (1995)
11. E. Sarid, 'The non-equilibrium anode plasma in a magnetically insulated high-voltage gap', Dissertation, Weizman Institute of Science, Rehovot, Israel (1990)
12. H. Bluhm, 'Die Erzeugung gepulster Megaampere-Ionenströme für die Materie- und Trägheitsfusionsforschung', FZKA 5528, Forschungszentrum Karlsruhe, 1995
13. M.Desjarlais, 'Theory of applied-B ion diodes', Phys. Fluids B, 1, 1709, 1989
14. T.D. Pointon, M.P. Desjarlais, 'Three-dimensional particle-in-cell simulations of applied-B ion diodes on the particle beam fusion accelerator II', J. Appl. Phys., 80, 2079, 1996.
15. A.V. Gretchikha, 'Applied-B ion diode theory: the screening scale, relaxation of a Lagrangian invariant, and the diode stability', Phys. Plasmas, 6, 316 (1999)
16. T.D.Pointon, O.Boine-Frankenheim, T.A.Mehlhorn. Proc. 13th Conf. on Laser Interaction and Related Plasma Phenomena, Monterey, 13-18 April 1997, AIP Conference Proceedings 406 (1997) 67

17. A. Friedman, S.E. Parker, S.L.Ray, and C.K. Birdsall, ‘Multi-scale particle-in-cell plasma simulation’, J. Comput. Phys. 96, 54 (1991)
18. P.W. Rambo and J. Denavit, ‘Time-implicit fluid simulation of collisional plasmas’, J. Comput. Phys. 98, 317 (1992)
19. I.S.Landman, H.Würz, ‘A lens model for applied-B ion diodes’, FZKA 6119, Forschungszentrum Karlsruhe, 1999
20. L.D.Landau, E.M.Lifshitz, ‘The classical theory of fields’, Pergamon Press, 1959
21. Burke P.G., Smith K. Rev. Mod. Phys., 34, 458 (1962)
22. Van Regemorter H. Astrophys. J., 132, 906 (1962)
23. W.L.Wiese, M.W.Smith, B.M.Glennon, ‘Atomic transition probabilities’, Vol. 1. NBS, Washington, D.C., 1966
24. D.J. Johnson et al., J. Appl. Phys., 52, 168 (1981)
25. I. Landman, H. Würz, ‘SFOREV a code for calculation of self-consistent radiation transfer’, FZKA report, to be published

Table 1. Electron energy losses for different kinds of collisions

E [kV/cm]	1	10	100	1000
elastic loss	0.68	0.02	0.001	$3\cdot10^{-4}$
excitations	0.29	0.59	0.5	0.6
ionization	0.03	0.39	0.5	0.4

Table 2. Final ion density, gap electron density and voltage delay time for operation with complete exhaustion of the quasineutral layer as function of the maximal voltage

φ_{max} (MV)	n_{imax}(cm^{-3})	n_{egap}(cm^{-3})	t_0 (ns)
1	$4.5\cdot10^{14}$	$2\cdot10^{12}$	15
2	$1.9\cdot10^{15}$	$5\cdot10^{12}$	32
5	$6.8\cdot10^{15}$	$1.3\cdot10^{12}$	50

Table 3. Comparison of experimental and numerical results

Physical parameters		**Experimental results**	**Numerical results**
T_e	(eV)	5 – 8	7 – 10
n_{egap}	(cm^{-3})	$2\cdot10^{13}$	$5\cdot10^{12}$
n_e	(cm^{-3})	$3\cdot10^{15} – 5\cdot10^{17}$	$5\cdot10^{14} – 7\cdot10^{15}$
l	(mm)	1 – 1.5	0.2 – 0.5
V_{exp}	(cm/μs)	2 – 5	1 – 3
V_i	(cm/μs)	3	1 – 2

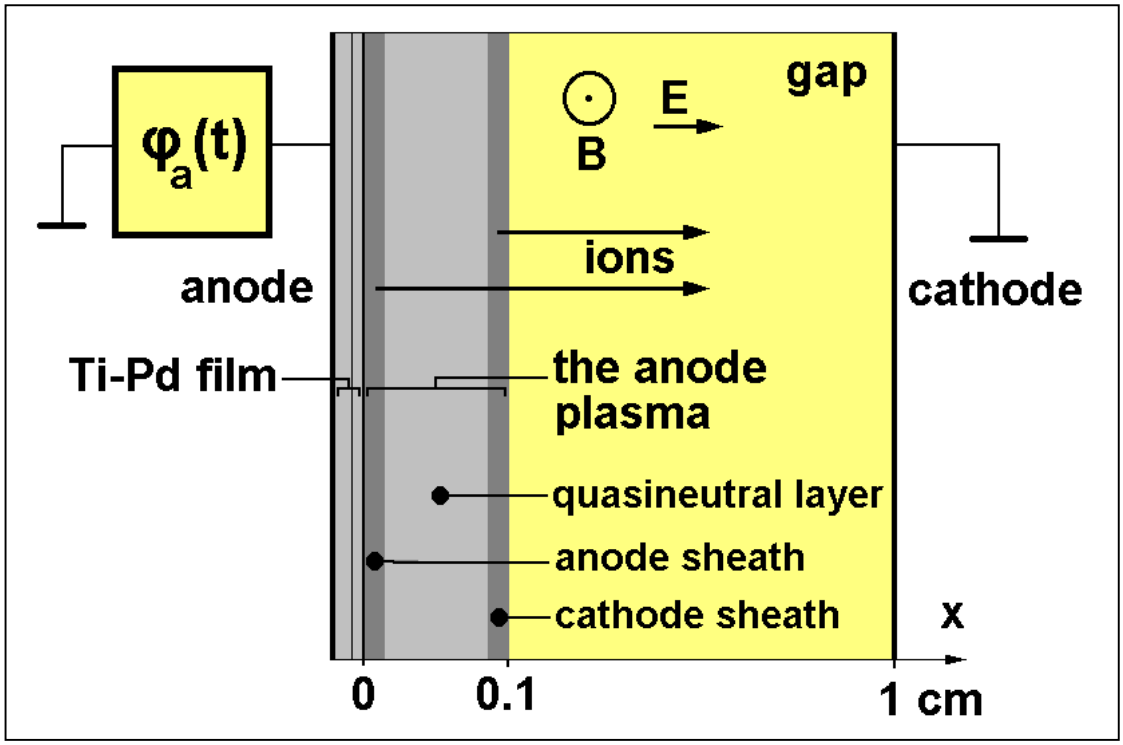

Fig. 1. 1 dim scheme of an applied-B ion diode with details of the anode plasma: the gas supplying Ti-Pd film, the applied magnetic field B, the voltage $\varphi_a(t)$ applied across the diode gap and ion beam production in the anode sheath and in the edge of the anode plasma.

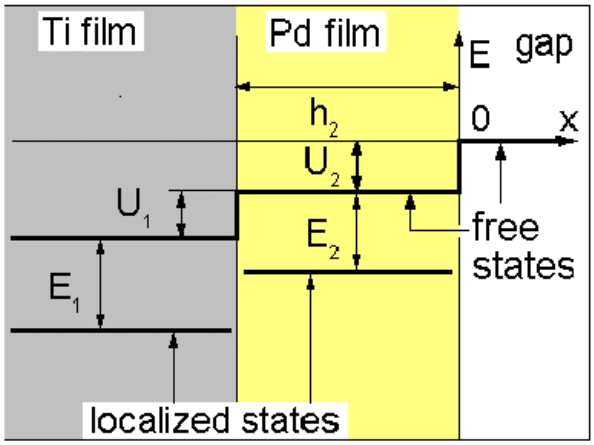

Fig. 2. Hydrogen energy states in the Ti-Pd structure at an anode plate

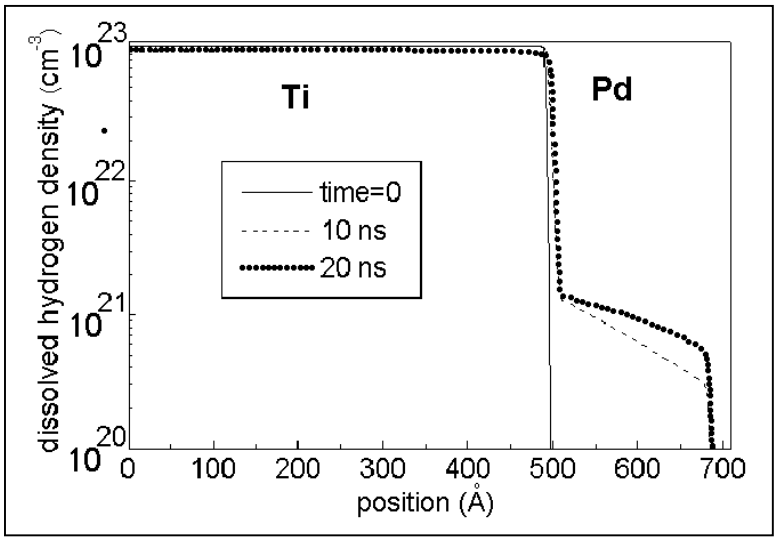

Fig. 3. Density distribution of hydrogen in the storage layer (0 – 500 Å) and in the transition layer (500 – 700 Å).

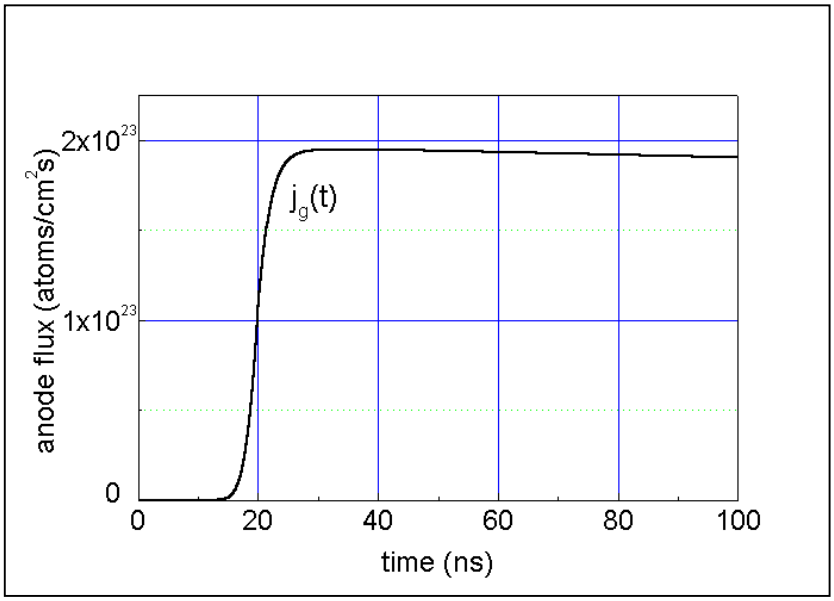

Fig. 4. Time dependence of the hydrogen particle flux j_g from the anode.

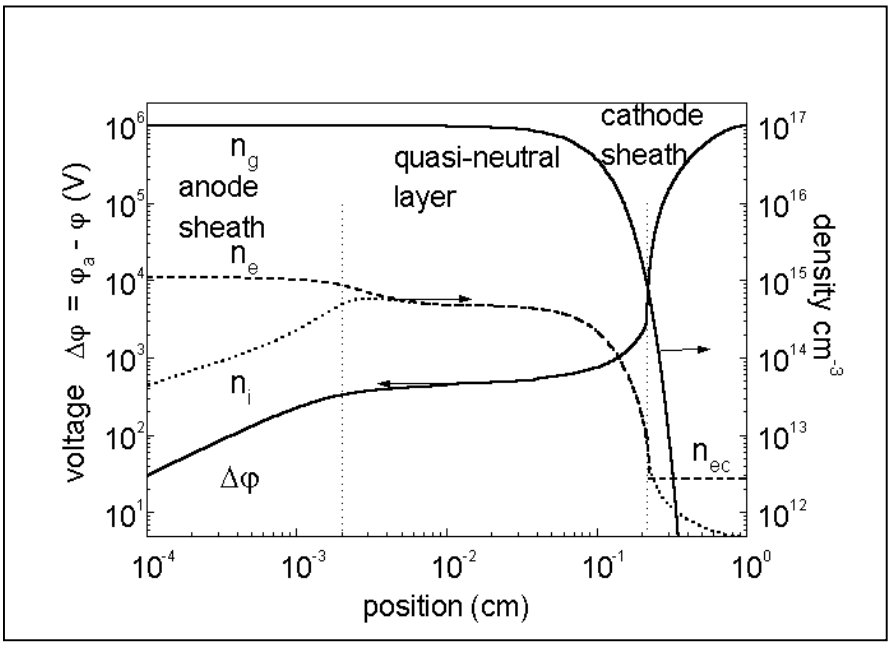

Fig. 5. Distribution of voltage and densities in the anode-cathode gap (hydrogen, B = 3 T)

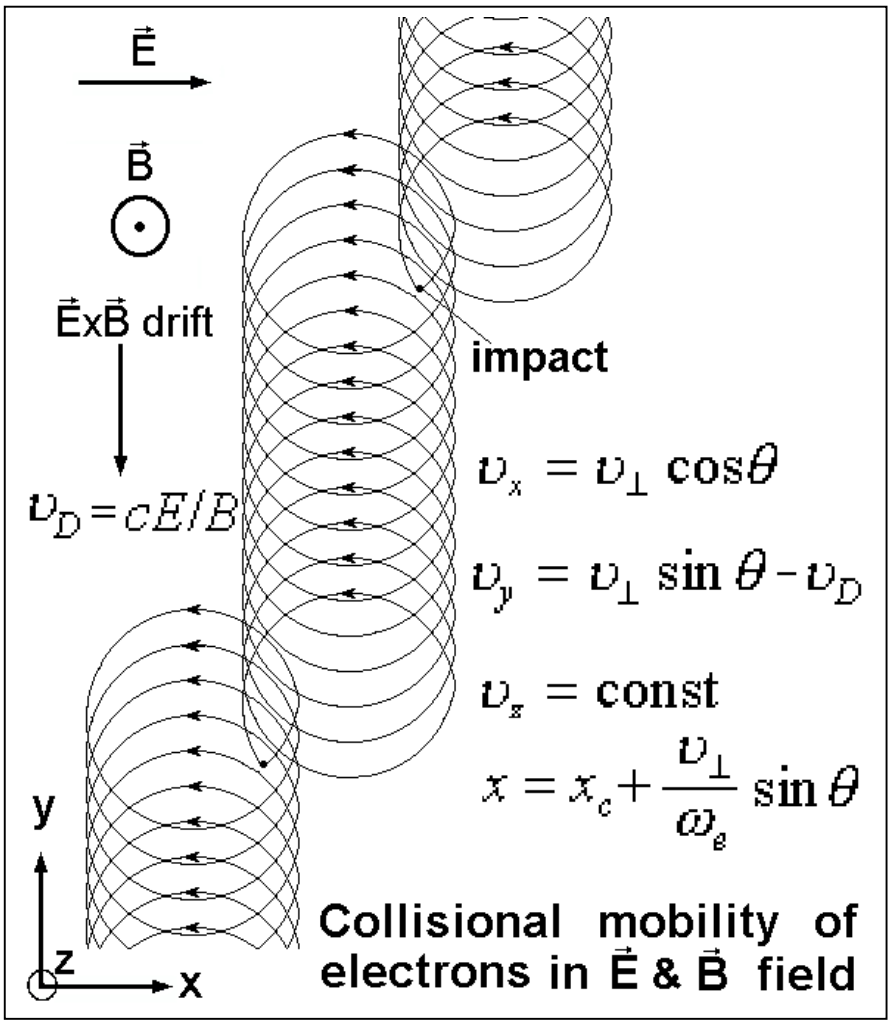

Fig. 6 The motion of electrons in crossed E and B fields

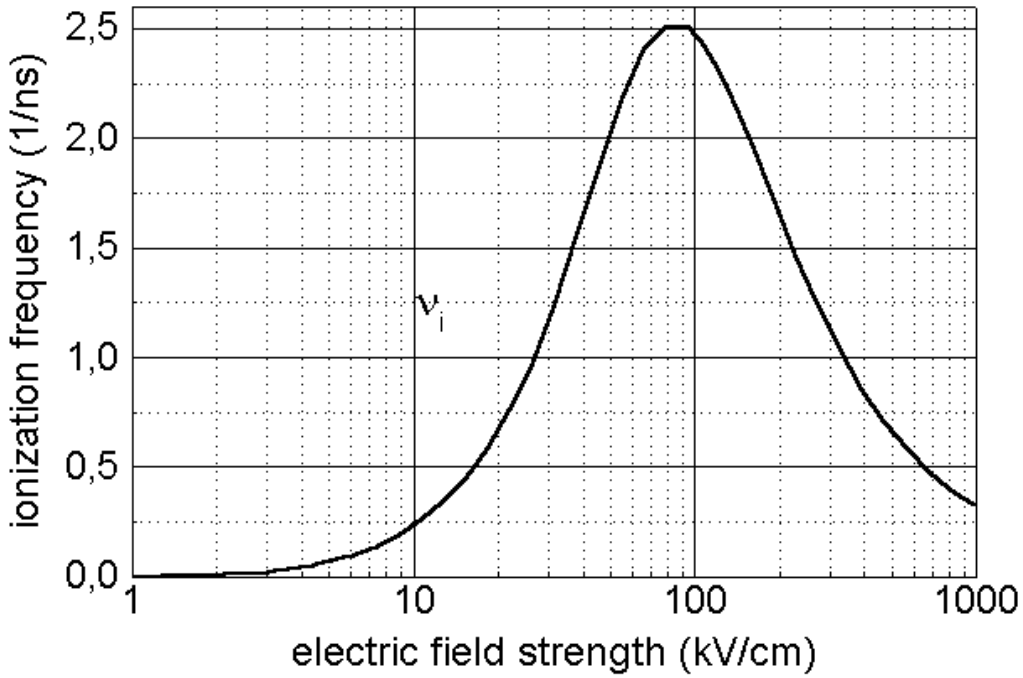

Fig. 7 Ionization frequency as function of the electric field strength (hydrogen, $n_g = 10^{17}$ cm^{-3} and $B = 3$ T)

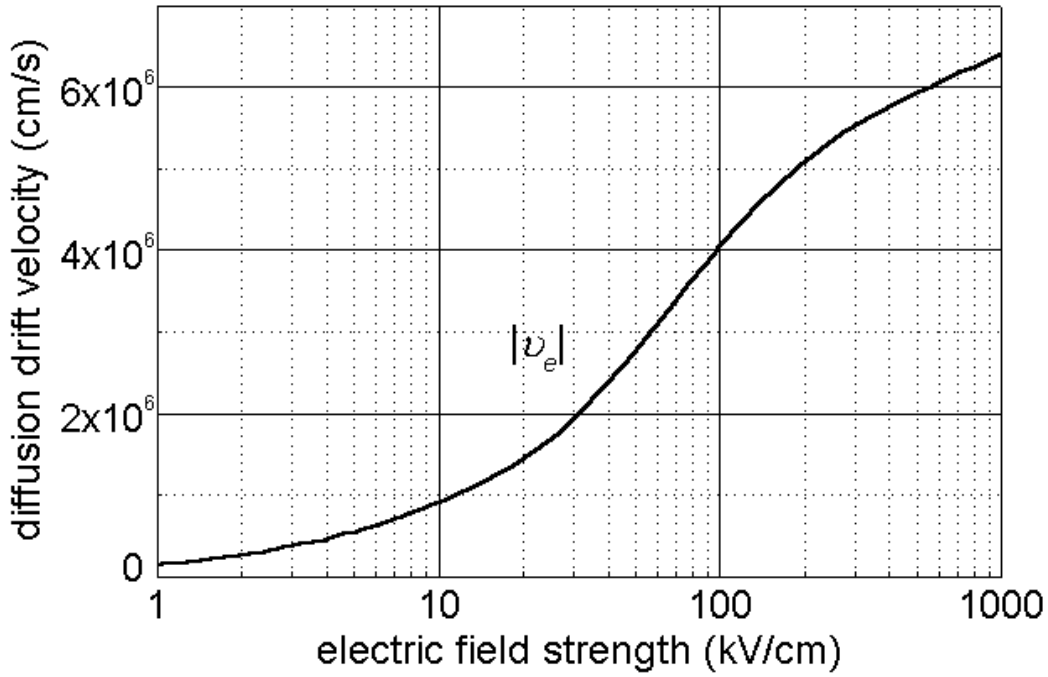

Fig. 8 Diffusion drift velocity of electrons as function of the electric field strength (hydrogen, $n_g = 10^{17}$ cm^{-3} and $B = 3$ T)

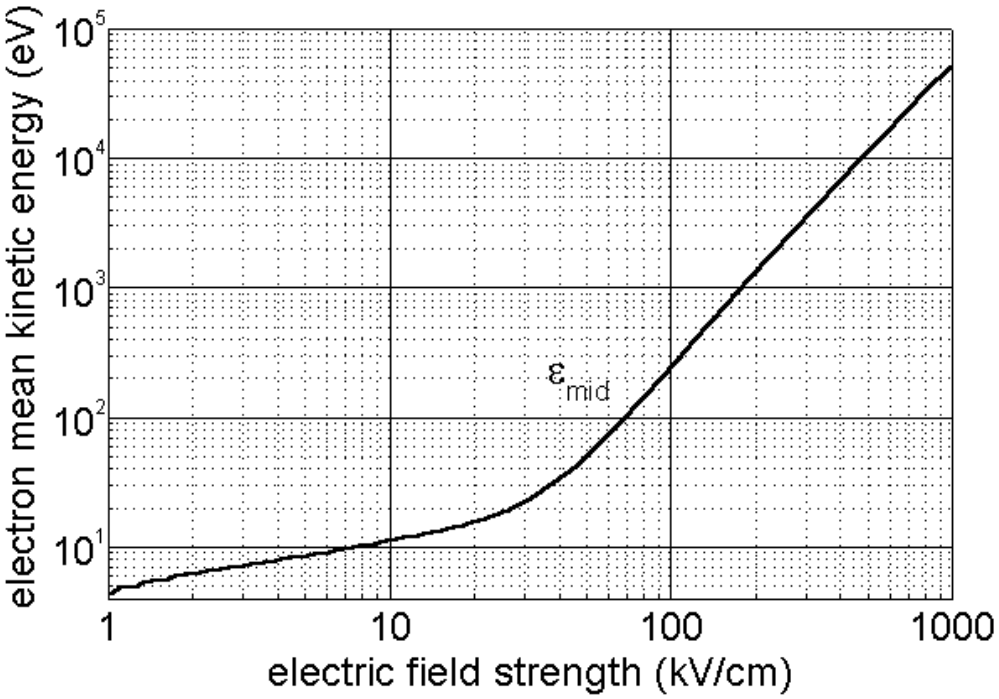

Fig. 9 Mean electron kinetic energy as function of the electric field strength (hydrogen, B = 3 T)

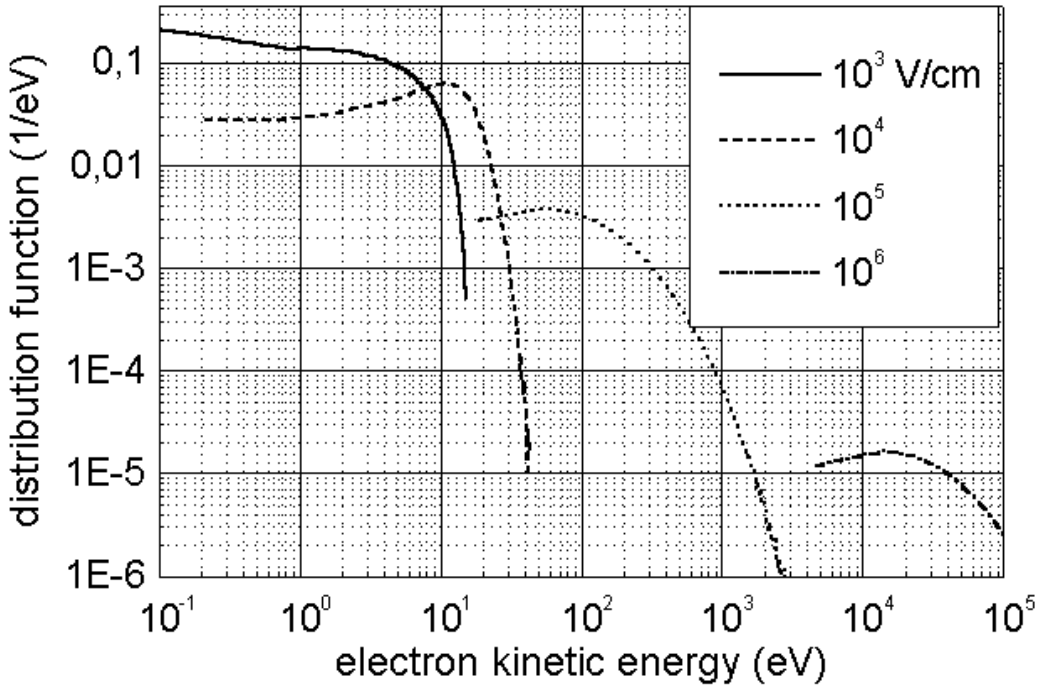

Fig. 10. Electron energy distribution function at different electric field strengths (hydrogen, B = 3 T)

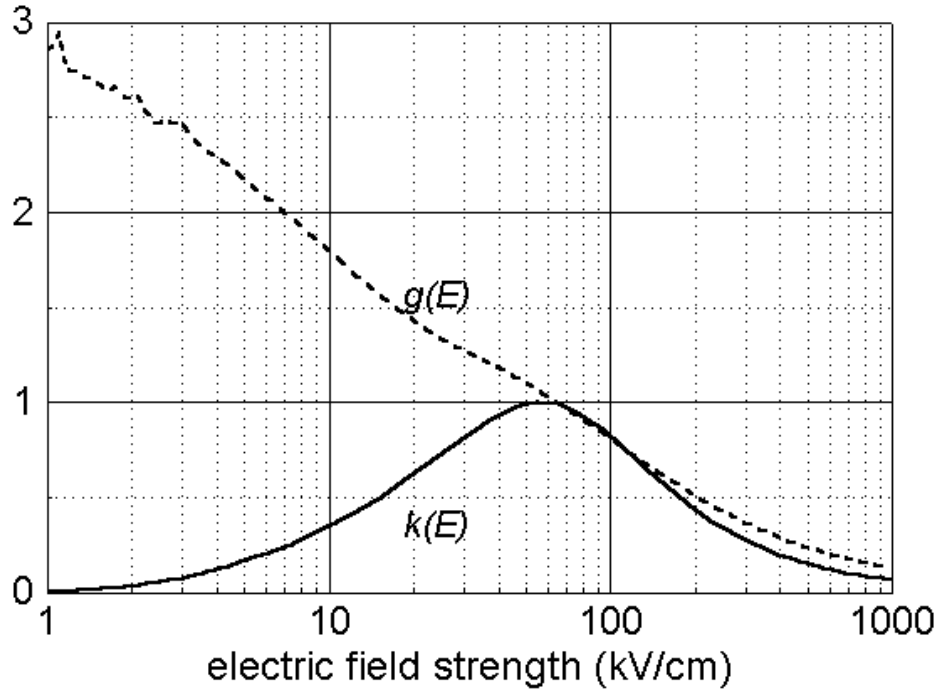

Fig. 11 The functions $k(E) = a\nu_i/\upsilon_e$ and $g(E) = |\upsilon_e|/\mu E$.

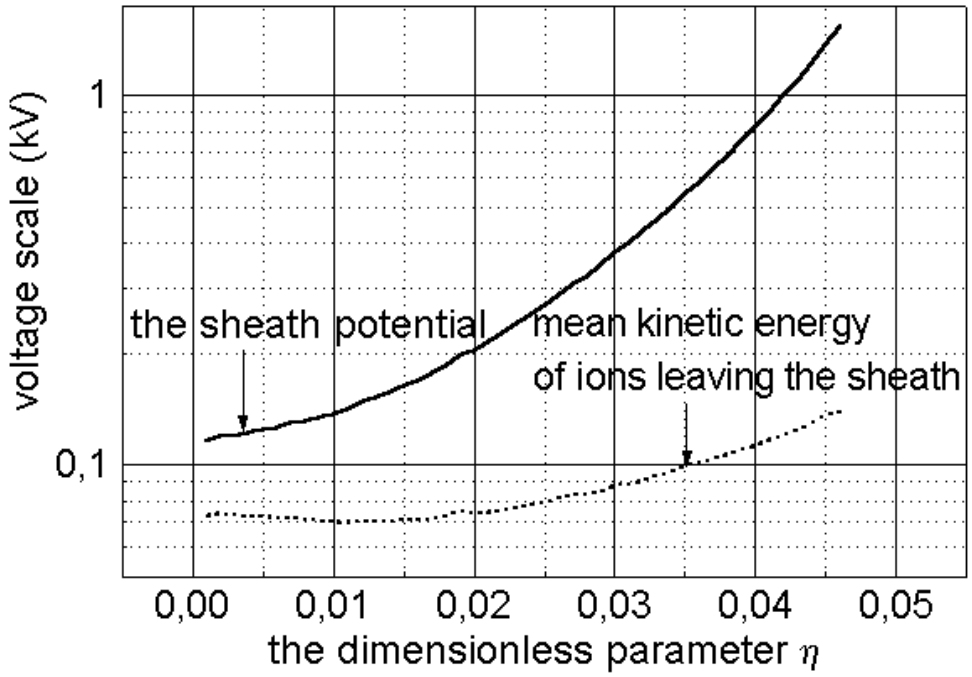

Fig. 12. Sheath potential $\Delta\varphi_a = \varphi_a - \varphi = \varphi^* u_\infty$ and mean kinetic energy of ions leaving the anode sheath as function of the parameter η.
(hydrogen, $n_g = 10^{17}$ cm^{-3} and $B = 3$ T)

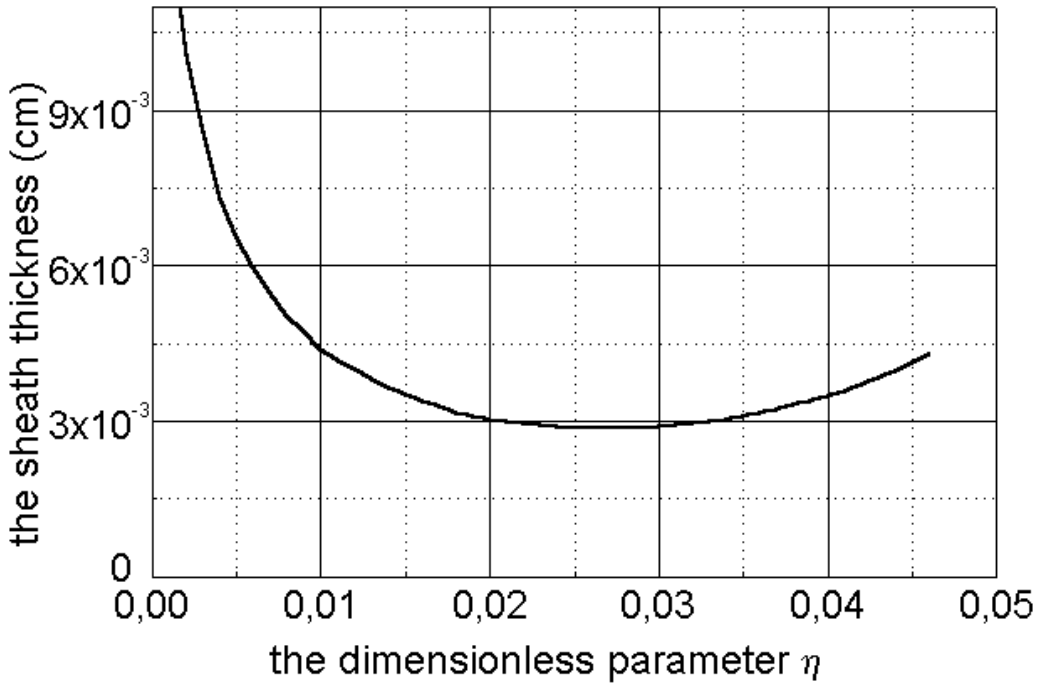

Fig. 13. Dependence of the anode sheath thickness on the parameter η.
(hydrogen, $n_g = 10^{17}$ cm^{-3} and $B = 3$ T)

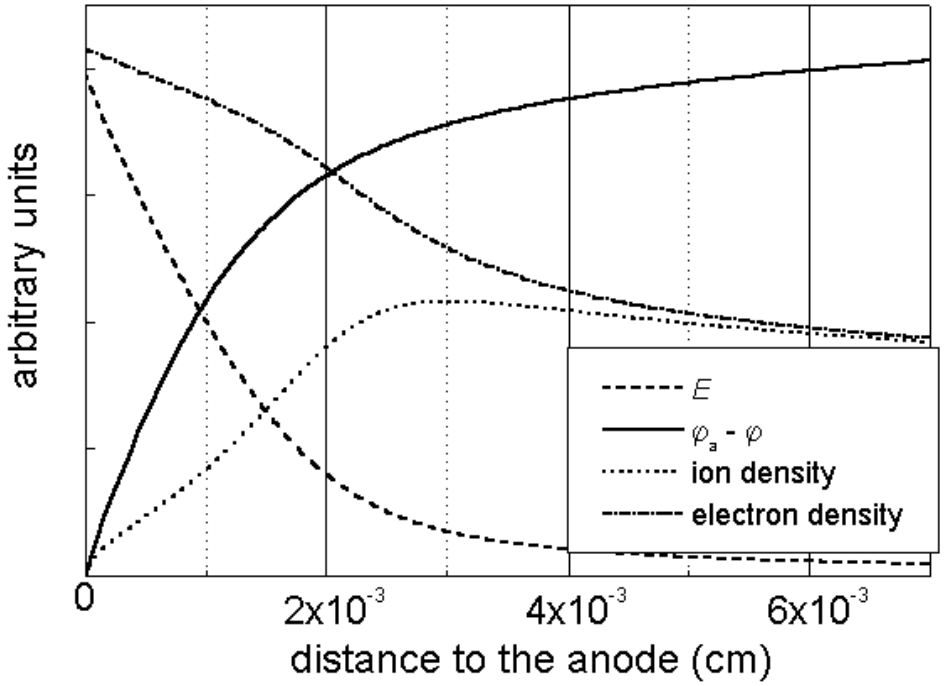

Fig. 14. The sheath structure for the case of $\eta = 0.028$
(hydrogen, $n_g = 10^{17}$ cm^{-3} and $B = 3$ T)

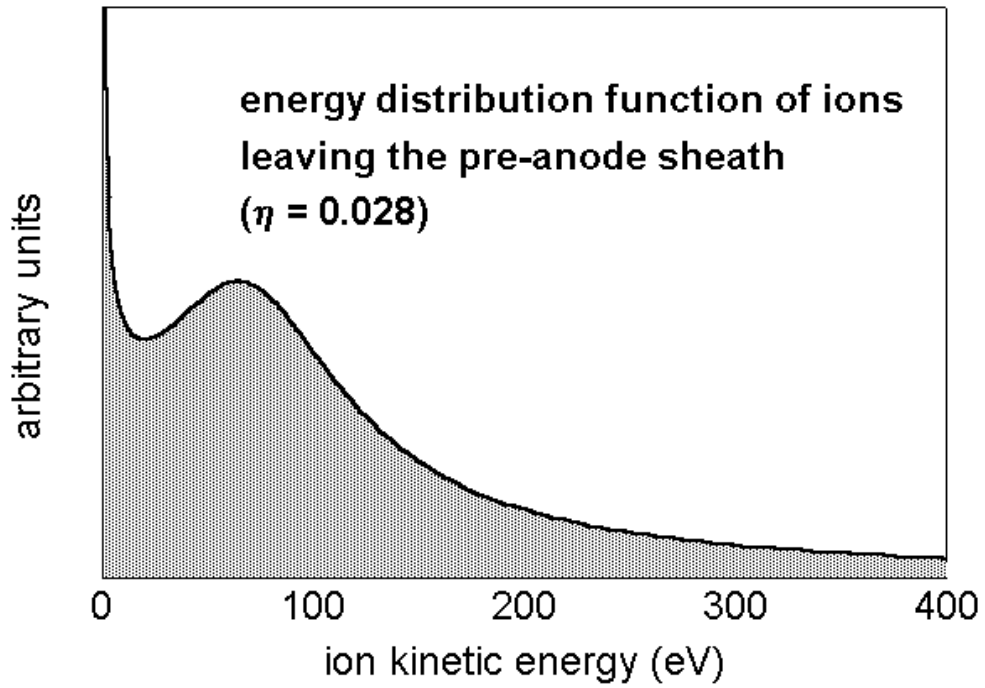

Fig. 15. The distribution function of ions produced and accelerated in the sheath.

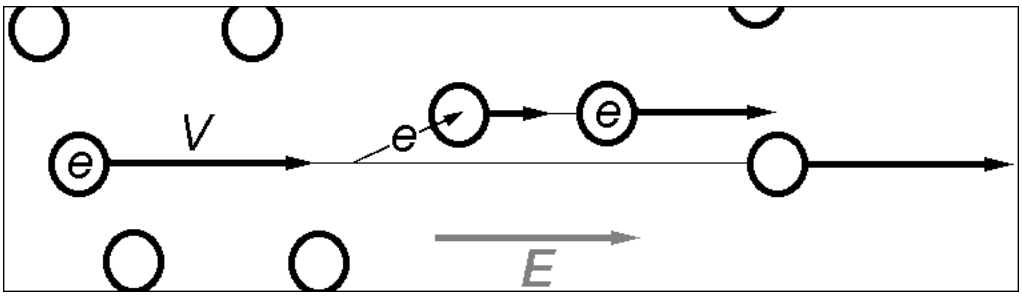

Fig. 16 Principal scheme of charge-exchange. Atoms are shown as circles. Positive charge *e* (simulating absence of the ionized electron) indicates an atom as ion. The charge jumps from the ion to a neutral at their rapprochement. Then the just charged atom accelerates in the electric field *E* while the discharged one continues to move with the previously acquired velocity.

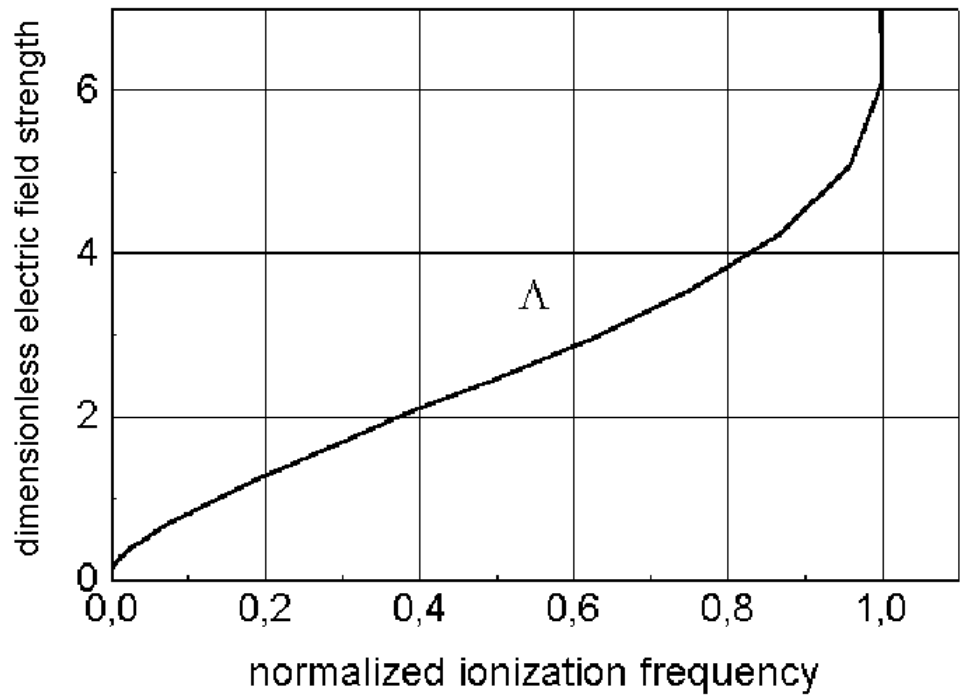

Fig. 17. The function $w = \Lambda(\nu_i/\nu_{i\max})$ reversed to the normalized ionization frequency (hydrogen, $n_g = 10^{17}$ cm^{-3} and $B = 3$ T)

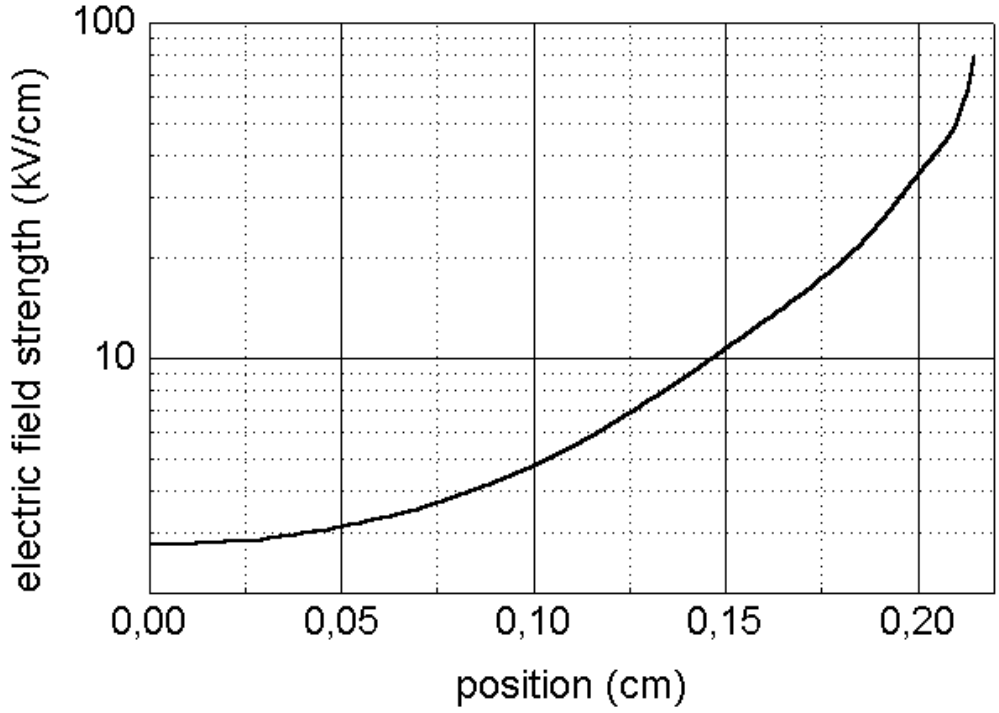

Fig. 18. Electric field strength in the quasineutral layer $E(x) = (\varphi^*/l)w(x/l)$. (hydrogen, $n_g = 10^{17}$ cm^{-3} and $B = 3$ T)

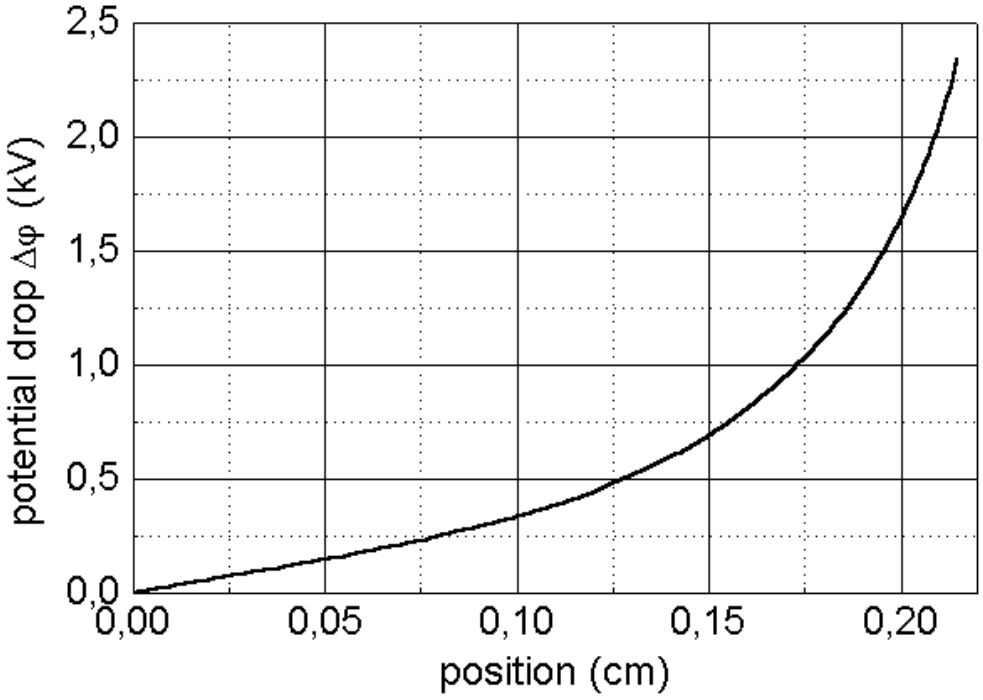

Fig. 19. Drop of the electric potential in the quasineutral layer.

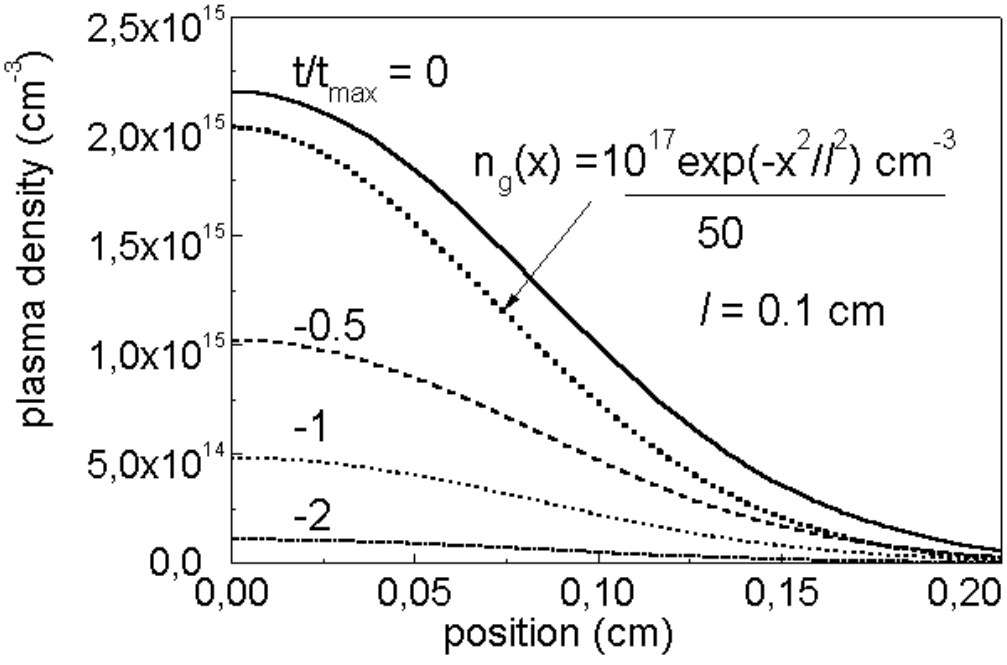

Fig. 20. Evolution of plasma density in the quasineutral layer.

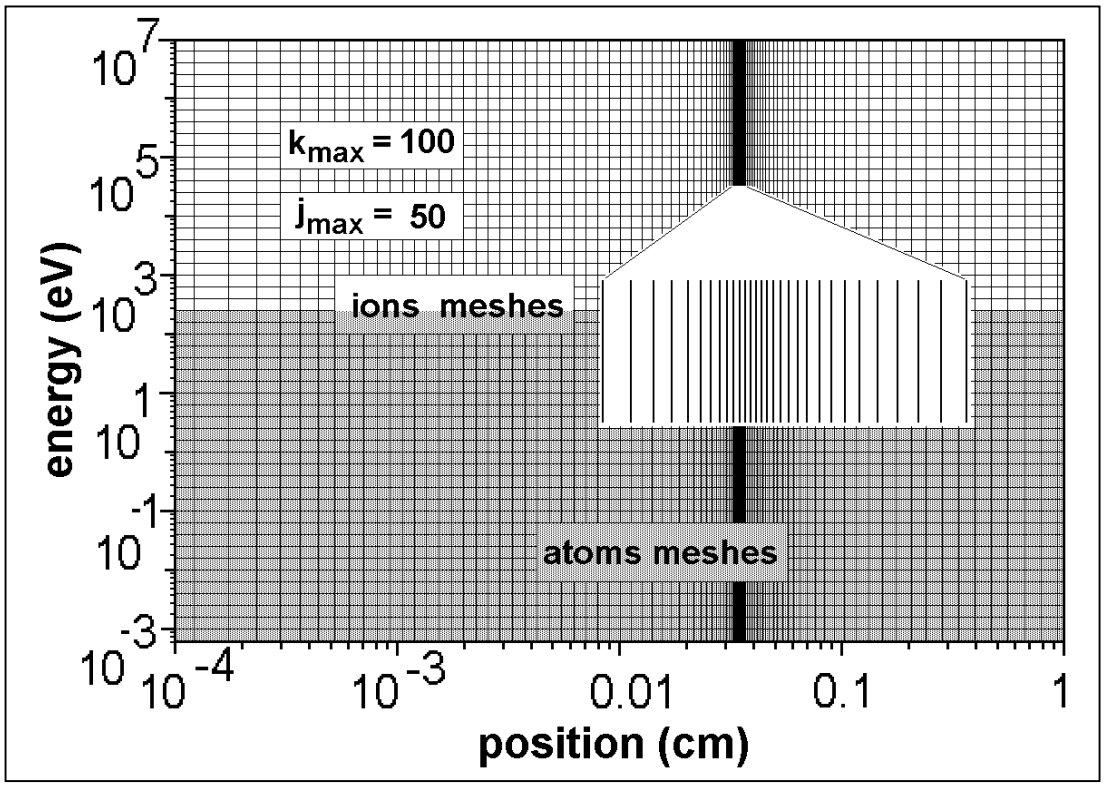

Fig. 21 The numerical grid schematically. Spatial mesh indexes j ($1 \le j \le j_{max}$). Velocity mesh indexes k ($1 \le k \le k_{max}$). It is logarithmic in v- and in x-directions except of the narrow region describing the cathode edge of the anode plasma.

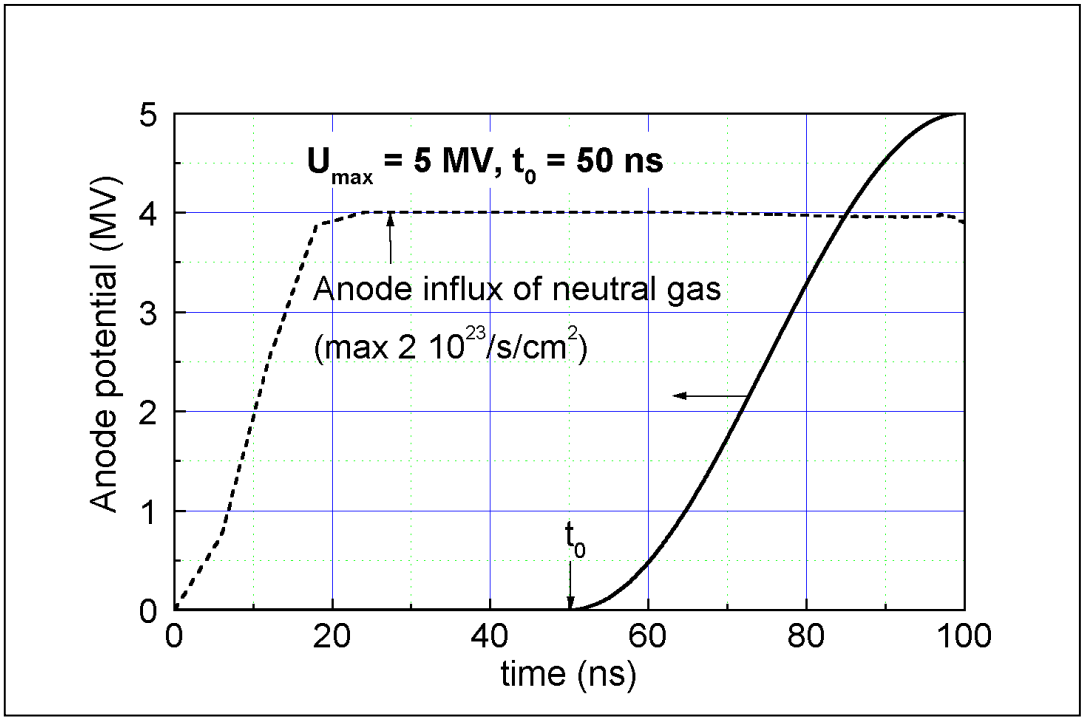

Fig. 22 Development of anode potential and gas influx from the Ti-Pd film. It is valid $U_{max} \equiv \varphi_{max}$.

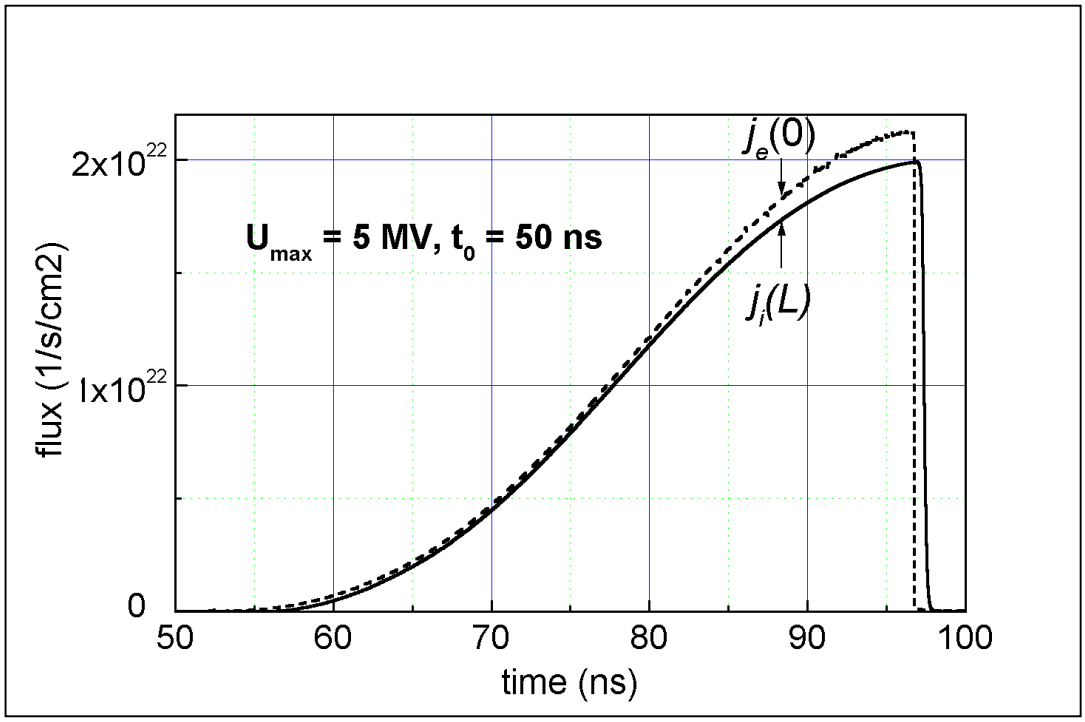

Fig. 23 Development of the electron flux onto the anode and the ion fluxes to the cathode. The final disruption of the fluxes corresponds to the exhaustion of the quasineutral layer near the anode.

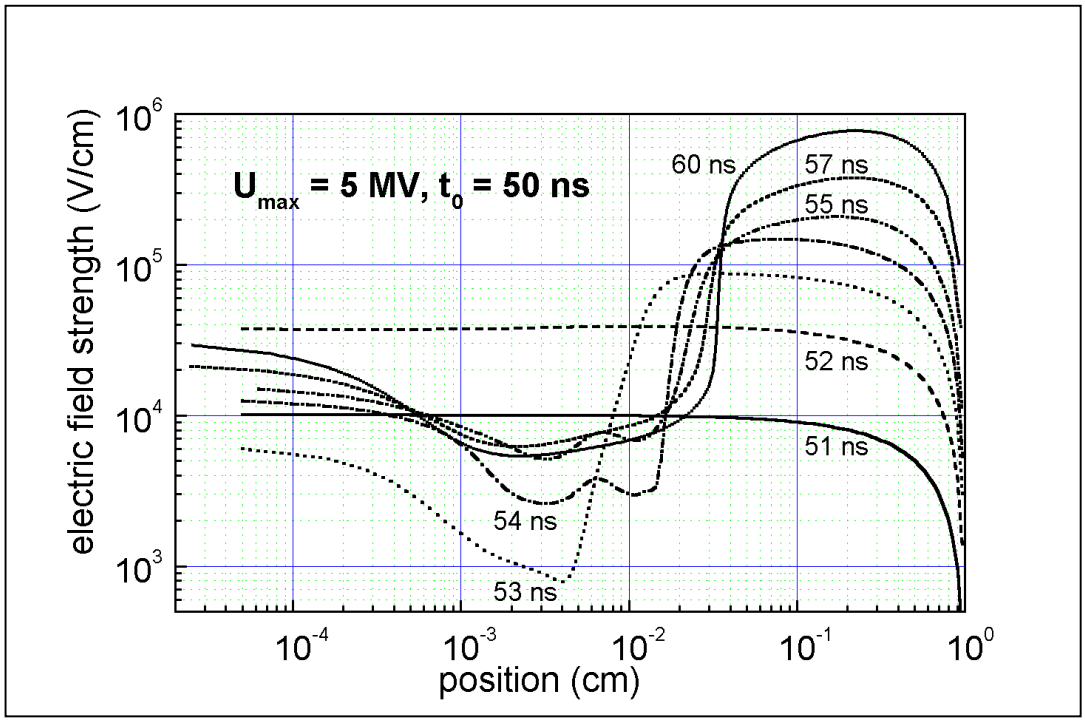

Fig. 24. Development of the electric field in the gap during the stage of formation of the self-consistent field and the quasineutral layer.

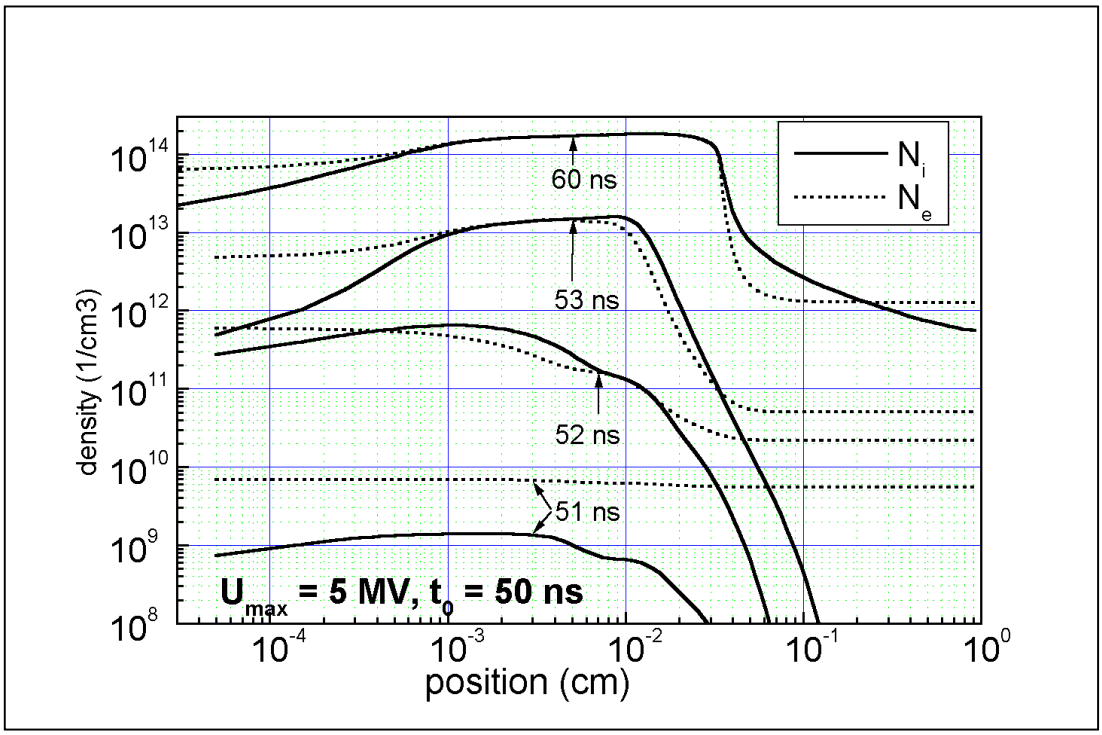

Fig. 25. Development of electron and ion densities in the gap during the stage of the quasineutral layer formation.

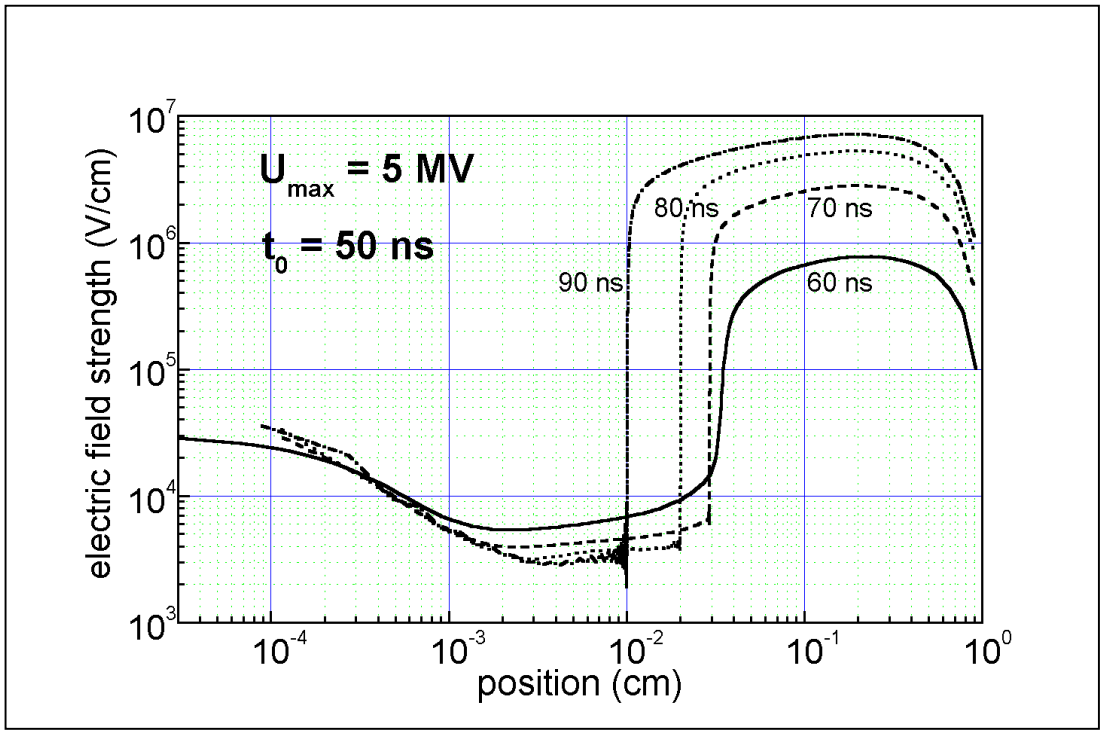

Fig. 26. Evolution of the electric field during the main phase of the diode operation. From the propagation of the position of the maximal field gradient towards the anode exhaustion of the quasineutral layer is evident. Near this position numerical oscillations develop.

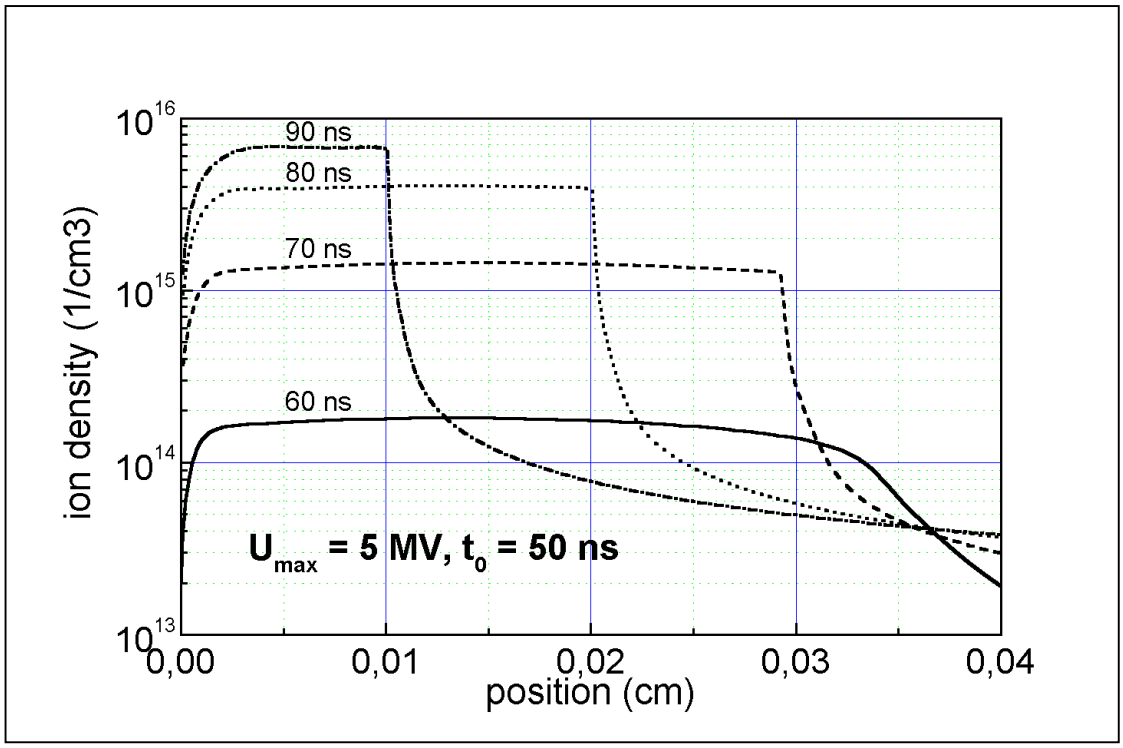

Fig. 27. Evolution of the ion density near the anode during the main stage of the diode operation. Exhaustion of the quasineutral layer is clearly seen as shift of the right edge of the ion density towards the anode.

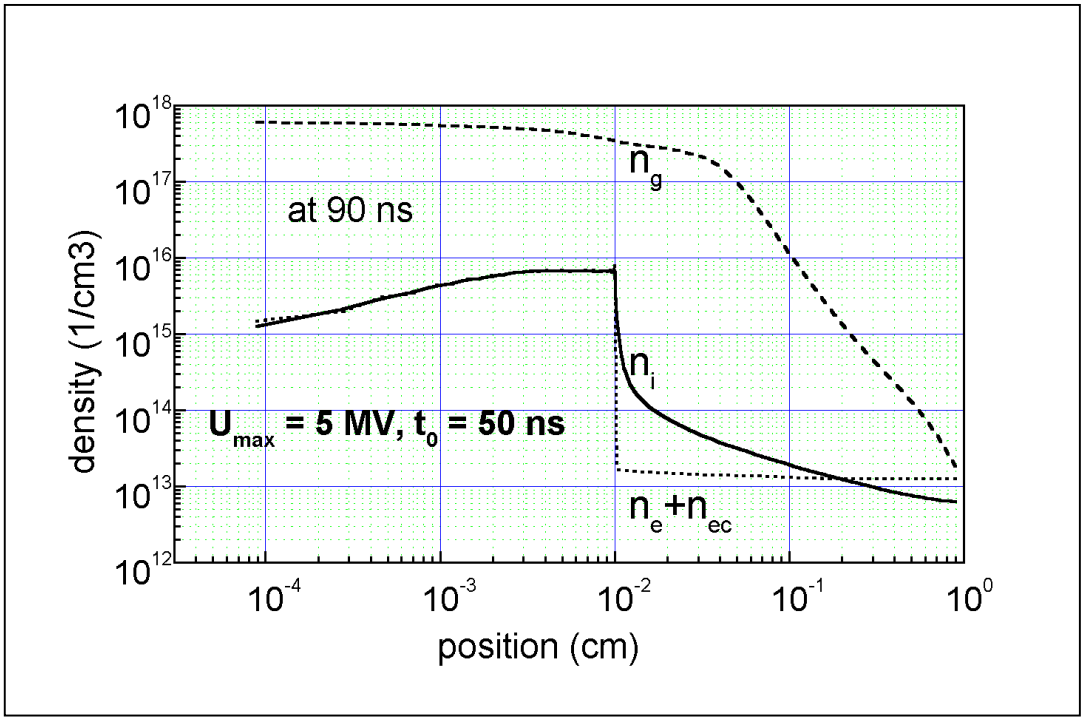

Fig. 28. Distribution of neutral gas density and densities of electrons and ions in the gap in the final phase of the diode operation. The quasineutrality fails in the pre-anode sheath and in the main volume of the gap. In the main volume the cathode electrons (n_{ec}) dominate over those produced by ionization (n_e).

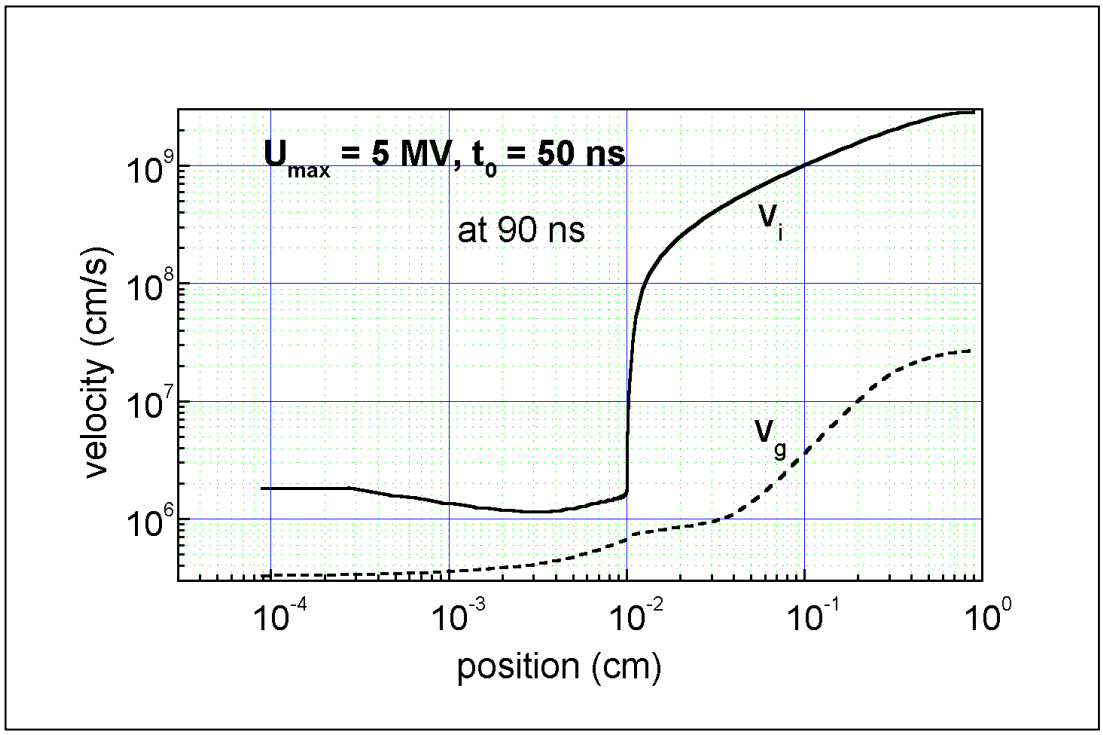

Fig. 29. Mean velocities of ions and of neutral atoms in the gap in the final phase of the diode operation. Maximal ion velocity corresponds to the kinetic energy of φ_{max}. Maximal atomic velocity corresponds to their kinetic energy of $5 \cdot 10^2$ eV.

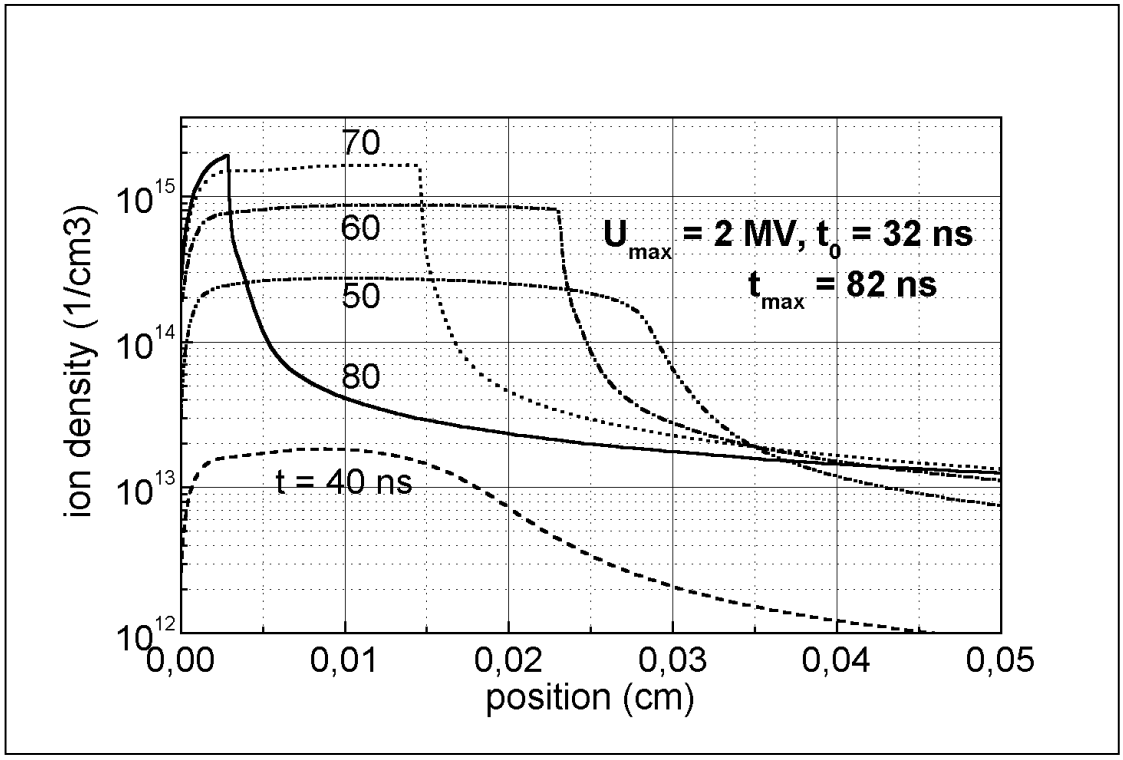

Fig. 30. Evolution of the ion density near the anode for U_{max} = 2 MV. The time t_{max} is the moment of reaching the maximal voltage: $\varphi_a(t_{max}) = U_{max}$.

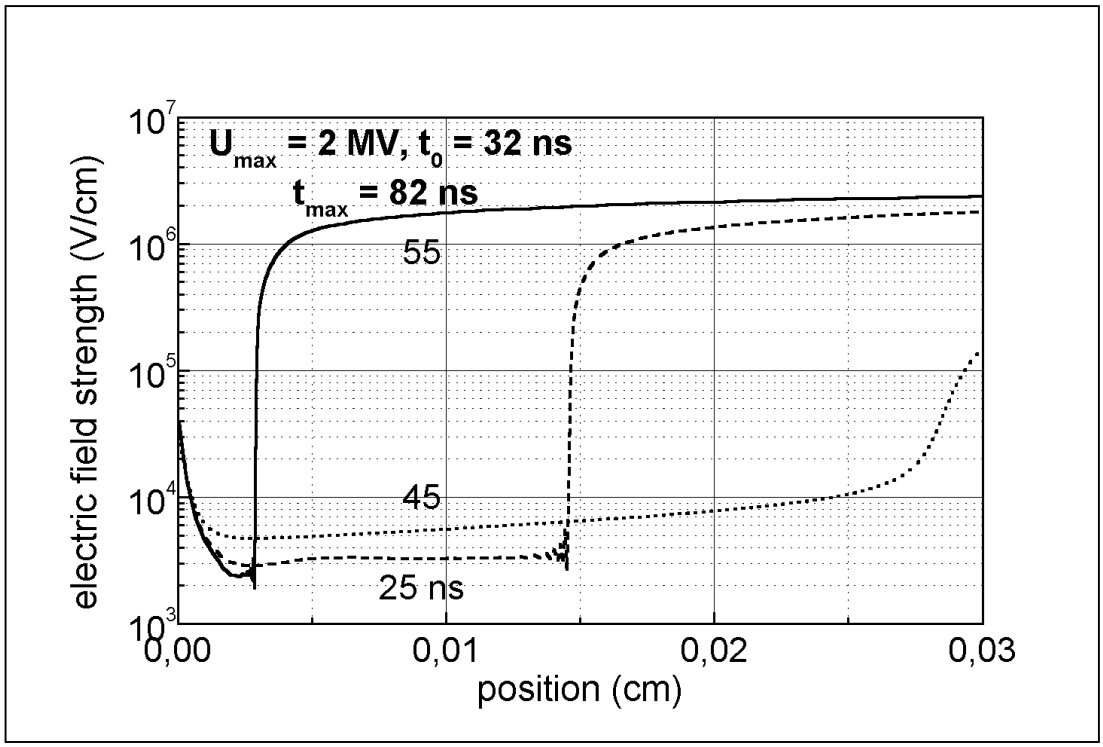

Fig. 31. Evolution of the electric field near the anode for U_{max} = 2 MV

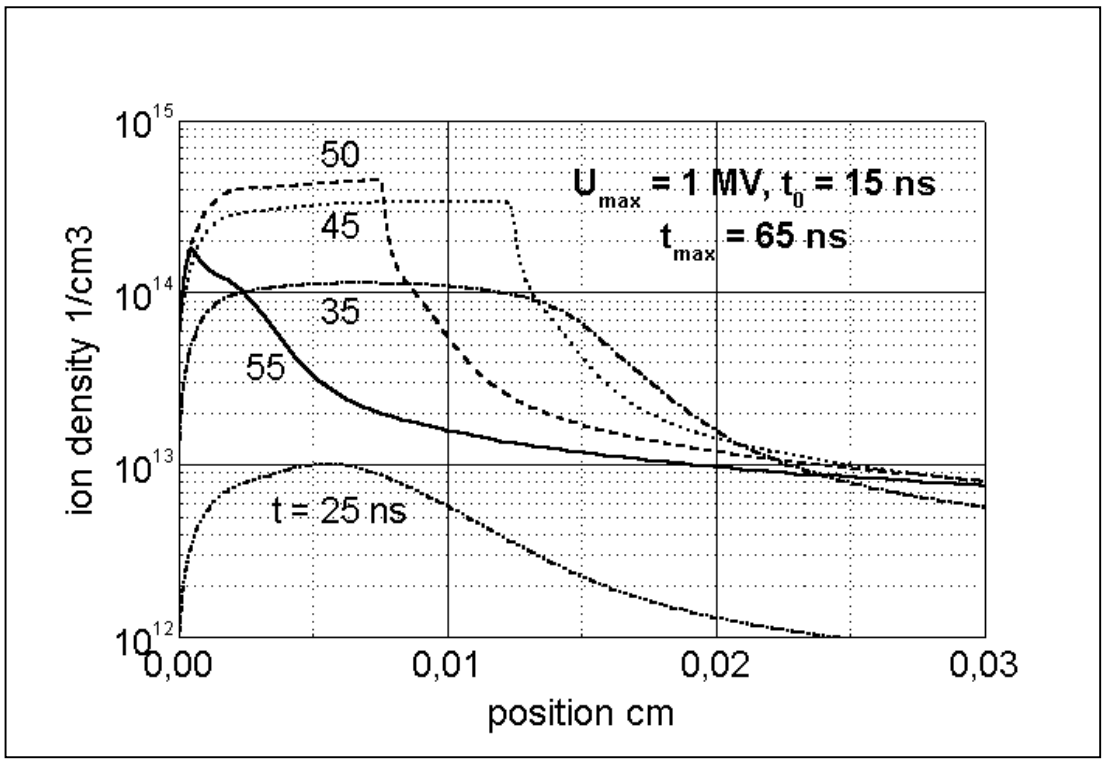

Fig. 32. Evolution of the ion density near the anode for U_{max} = 1 MV.

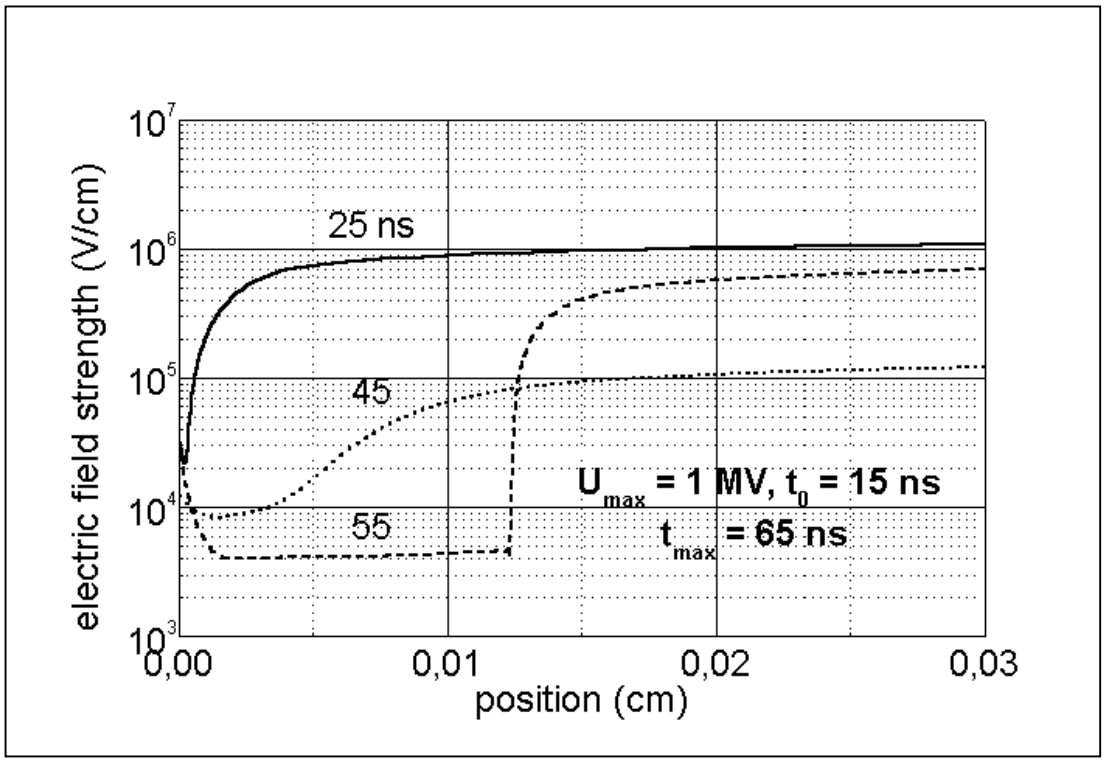

Fig. 33 Evolution of the electric field near the anode for U_{max} = 1 MV

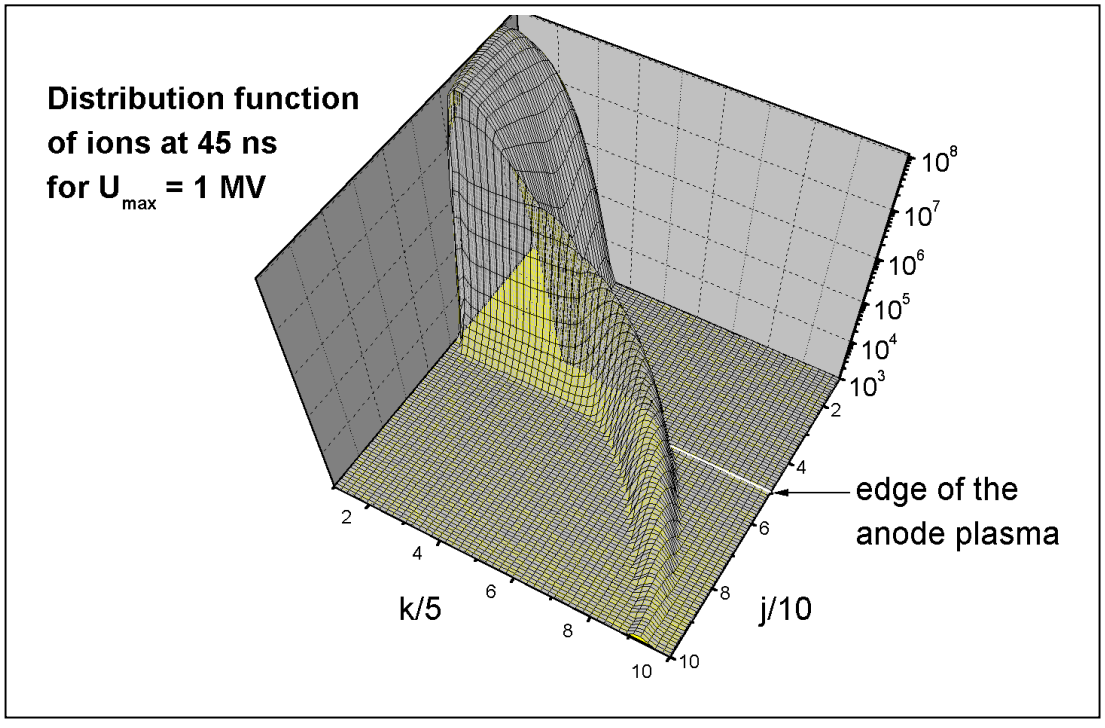

Fig. 34. Typical ion distribution in the gap. The v-axis is represented by the mesh indexes k divided by 5. The x-axis is represented by the mesh indexes j divided by 10.

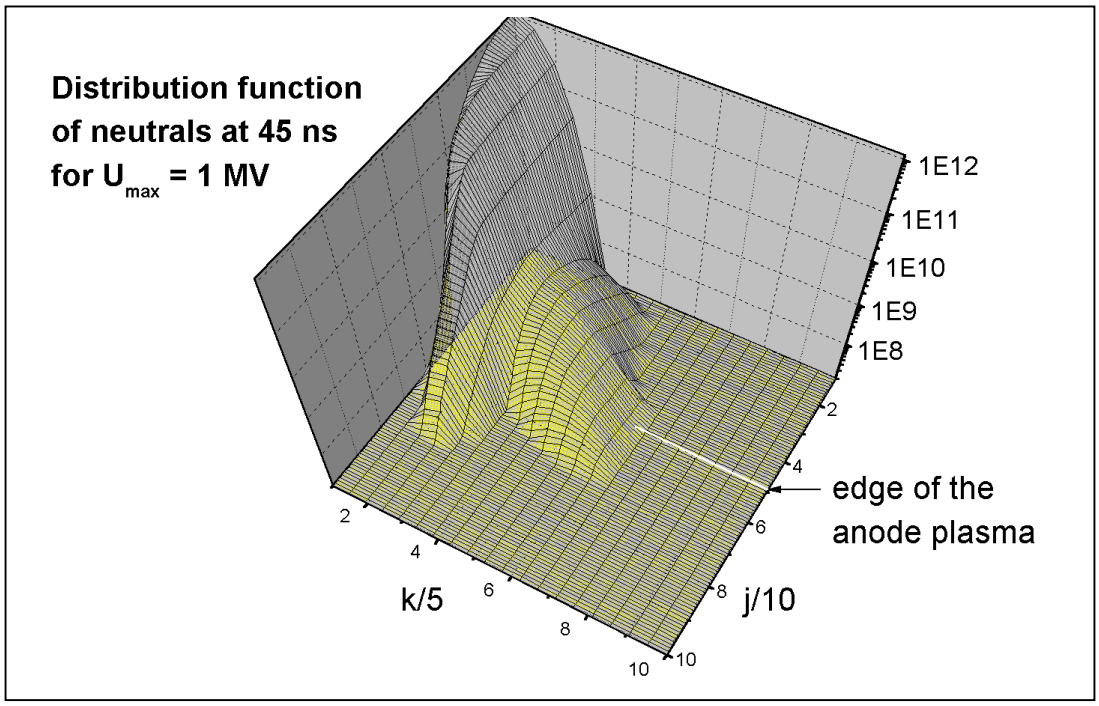

Fig. 35 Typical distribution of neutral atoms in the gap. The υ-axis is represented by the mesh indexes k divided by 5. The x-axis is represented by the mesh indexes j divided by 10.

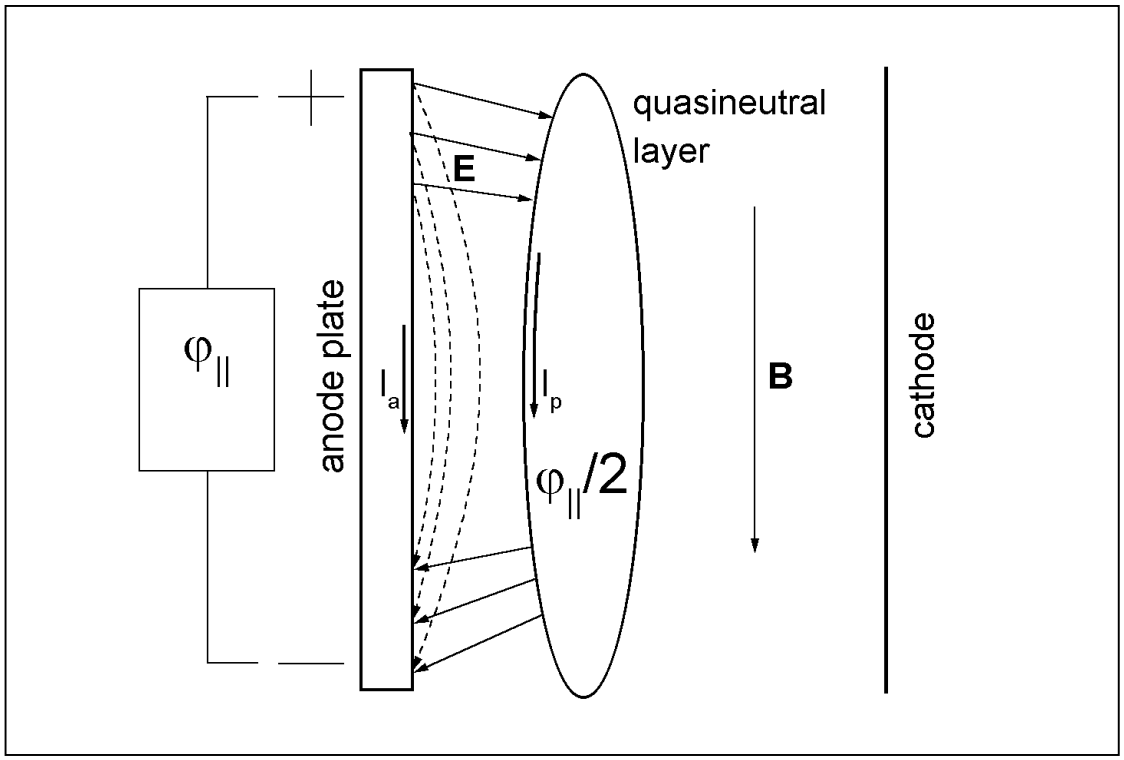

Fig. 36 Typical spatial distribution of electric field at the early stage of the pre-anode discharge (the dashed lines of the field **E**) and at the developed stage with formed quasineutral layer (the solid field lines).